Non-fullerene acceptors for organic solar cells

*Cenqi Yan[1], Stephen Barlow[2], Zhaohui Wang[3], He Yan[4], Alex K.-Y. Jen[5], Seth R. Marder[2] and Xiaowei Zhan[1]**

Abstract | Non-fullerene acceptors (NFAs) are currently a major focus of research in the development of bulk-heterojunction organic solar cells (OSCs). In contrast to the widely used fullerene acceptors (FAs), the optical properties and electronic energy levels of NFAs can be readily tuned. NFA-based OSCs can also achieve greater thermal stability and photochemical stability, as well as longer device lifetimes, than their FA-based counterparts. Historically, the performance of NFA OSCs has lagged behind that of fullerene devices. However, recent developments have led to a rapid increase in power conversion efficiencies for NFA OSCs, with values now exceeding 13%, demonstrating the viability of using NFAs to replace FAs in next-generation high-performance OSCs. This Review discusses the important work that has led to this remarkable progress, focusing on the two most promising NFA classes to date: rylene diimide-based materials and materials based on fused aromatic cores with strong electron-accepting end groups. The key structure–property relationships, donor–acceptor matching criteria and aspects of device physics are discussed. Finally, we consider the remaining challenges and promising future directions for the NFA OSCs field.

[1]*Department of Materials Science and Engineering, College of Engineering, Key Laboratory of Polymer Chemistry and Physics of Ministry of Education, Peking University, Beijing, China.*
[2]*School of Chemistry and Biochemistry, and Center for Organic Photonics and Electronics, Georgia Institute of Technology, Atlanta, GA, USA.*
[3]*MOE Key Laboratory of Organic Optoelectronics and Molecular Engineering, Department of Chemistry, Tsinghua University, Beijing, China.*
[4]*Department of Chemistry and Hong Kong Branch of Chinese National Engineering Research Center for Tissue Restoration and Reconstruction, Hong Kong University of Science and Technology, Clear Water Bay, Kowloon, Hong Kong, China.*
[5]*Department of Materials Science and Engineering, The City University of Hong Kong, Hong Kong, China.*
**e-mail: xwzhan@pku.edu.cn*

doi:10.1038/natrevmats.2018.3
Published online 13 Feb 2018

Conventional organic solar cells (OSCs) are typically based on blends of electron-donor materials and fullerene-based electron-acceptor materials (fullerene acceptors, FAs) that form bulk heterojunctions (BHJs) in devices (FIG. 1a). However, the focus in the development of OSCs has recently shifted to organic non-fullerene acceptors (NFAs) owing to several attractive properties of NFAs. In this Review, we first introduce the principles of OSC operation and then compare the advantages and drawbacks of FAs and NFAs. The discussion of solution-processed NFA-based OSCs is focused on the two major classes of NFAs that have led to notable advances in device performance. We then consider several aspects of device physics and, finally, provide a perspective on the challenges and future directions for the field.

Organic solar cells

Photovoltaic cells generate electrical power from solar energy. Although various technologies exist, including conventional as well as emerging quantum dot and perovskite solar cells, OSCs offer unique advantages for specific applications. For example, OSC panels can be fabricated through low-cost solution processes using environmentally friendly materials. OSCs are also lightweight, flexible and semi-transparent and can be scaled for use in large-area devices[1–3]. Moreover, their energy payback times — that is, the operation times needed to recover the energy expended in device fabrication — are substantially shorter than those of single-crystal silicon solar cells[4].

All solar cells absorb solar radiation, and the resulting excited states (excitons) dissociate into separated (non-Coulombically bound) holes and electrons. The feasibility of dissociation is dependent on the exciton binding energy, E_b, defined according to:

$$E_b = \mathrm{IE} - \mathrm{EA} - E_{op} \quad (1)$$

where IE – EA (the difference between the solid-state ionization energy and electron affinity) is the energy required to form a pair of separated charges from the ground state and E_{op} is the energy of the relaxed exciton relative to the ground state. EA is defined here as the energy released on the capture of an electron; thus, EA is positive for any organic electronic material in the solid state. In many inorganic materials, E_b is small (for example, $E_b \approx 15$ meV for silicon) and is easily overcome by thermal energy (25.85 meV at 300 K). By contrast, organic materials exhibit large E_b values (for example, $E_b \approx 0.7$ eV for poly(3-hexylthiophene) (P3HT)[5]), which leads to very inefficient charge separation in single-component organic materials. To achieve successful charge separation, OSCs rely on an active layer composed of an electron-rich ('donor', D) material and an electron-poor ('acceptor', A)

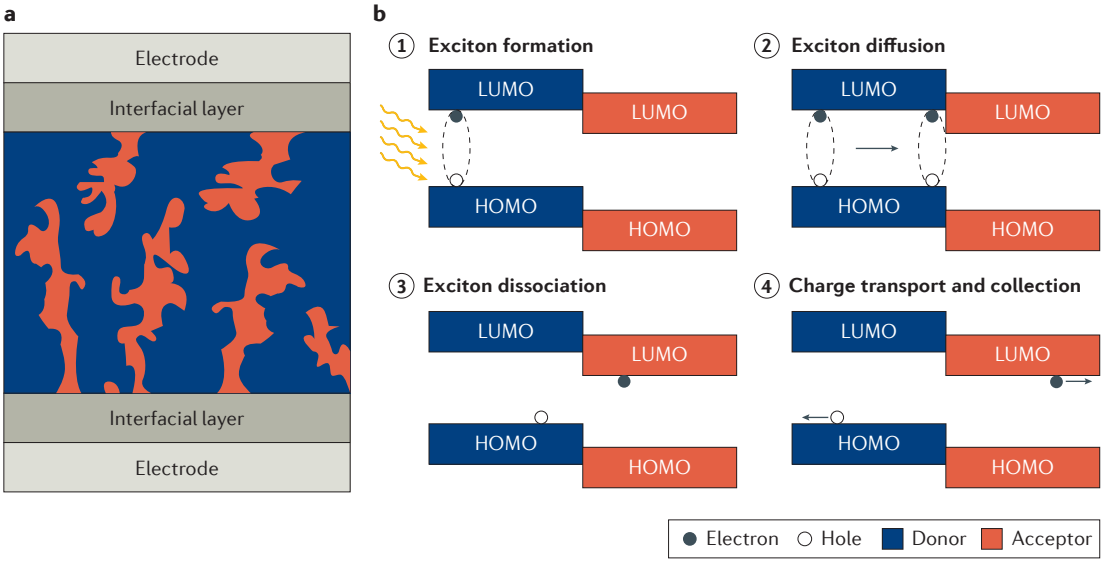

Figure 1 | **The structure and working mechanism of a bulk-heterojunction organic solar cell. a** | The structure of a bulk-heterojunction (BHJ) solar cell. In an ideal BHJ structure, donor and acceptor materials undergo nanoscale phase separation and form bicontinuous interpenetrating networks with large donor–acceptor interfacial areas. The red and blue regions represent the acceptor and donor domains, respectively. The variety of materials that are used as interfacial layers is very broad and includes metals, metal oxides, salts, polymer blends, organic acids, small molecules and conjugated compounds. Interfacial layers can function as charge-blocking layers, charge-transport layers and optical spacers and can form ohmic contacts with the electrode and active layer. **b** | Schematic showing the working mechanism of a BHJ solar cell for the case of donor excitation. First, photoexcitation of the donor generates a Coulomb-correlated electron–hole pair, known as an exciton. The exciton then diffuses to the donor–acceptor interface, where the exciton dissociates to form a geminate pair. The free charges are then transported and collected at the respective electrodes. The process of acceptor excitation is similar and, especially for non-fullerene acceptors, can be of comparable importance for generating current. HOMO, highest occupied molecular orbital; LUMO, lowest unoccupied molecular orbital.

material. These materials are chosen so that there is a driving force, $-\Delta G_{CS}$, for charge separation. In other words, the exciton dissociation should be exergonic so that:

$$\Delta G_{CS} = IE_{(D)} - EA_{(A)} - E_{op} - T\Delta S_{CS} < 0 \quad (2)$$

where E_{op} applies to the material with the lowest-energy absorption and ΔS_{CS} is the entropy of charge separation (which is often regarded as negligible and is therefore rarely considered). Combining equation 1 with equation 2 and neglecting $T\Delta S_{CS}$ for $E_{op(D)} < E_{op(A)}$ gives:

$$EA_{(A)} - EA_{(D)} > E_{b(D)} \quad (3)$$

which is essentially equivalent to the widely stated requirement for an offset in the energies of the lowest unoccupied molecular orbitals (LUMOs) of the donor and acceptor materials. Note that in cases in which $EA_{(D)}$ is estimated from $IE_{(D)} - E_{op(D)}$, E_b is already accounted for, and the LUMO–LUMO offset is equivalent to the driving force. Similarly, if $E_{op(A)} < E_{op(D)}$ (as is the case for many donor–NFA blends):

$$IE_{(A)} - IE_{(D)} > E_{b(A)} \quad (4)$$

Excitons diffuse to the donor–acceptor interface where they can form charge-transfer states that can then dissociate into free holes and electrons. The holes and electrons are transported through the donor-rich and acceptor-rich phases, respectively, to the relevant electrode, where they are collected (FIG. 1b). The first donor–acceptor OSCs were planar bilayer structures that were fabricated using an evaporation method; however, the exciton diffusion lengths for many organic materials are much shorter than the film thicknesses required for efficient light absorption. Along with the convenience of solution processing, this has led to the use of BHJs (FIG. 1a), in which the donor and acceptor are co-deposited from solution and, at least ideally, form bicontinuous interpenetrating donor and acceptor networks that provide hole and electron pathways, respectively. Moreover, BHJs also allow for thick films in which all excitons are formed close to a donor–acceptor interface[6] (FIG. 1).

The power conversion efficiency (PCE) is given by:

$$PCE = J_{SC} V_{OC} FF / P_{in} \quad (5)$$

where P_{in} is the power density of the incident solar radiation, J_{SC} is the short-circuit current density, V_{OC} is the open-circuit voltage and FF is the fill factor (defined as $P_{max}/(J_{SC}V_{OC})$, where P_{max} is the maximum power density). J_{SC} is limited by the rate at which the donor and acceptor materials absorb photons, the efficiency of exciton dissociation and the efficiencies with which the resultant charges are transported to and collected at the electrodes. The V_{OC} is limited by the energy of the interfacial donor–acceptor charge-transfer excited state, E_{CT}, given by:

$$E_{CT} = IE_{(D)} - EA_{(A)} - E_{b(CT)} \quad (6)$$

where $E_{b(CT)}$ is the exciton binding energy for this charge-transfer state[7], which corresponds to the Coulombic attraction between D^+ and A^- (and is much

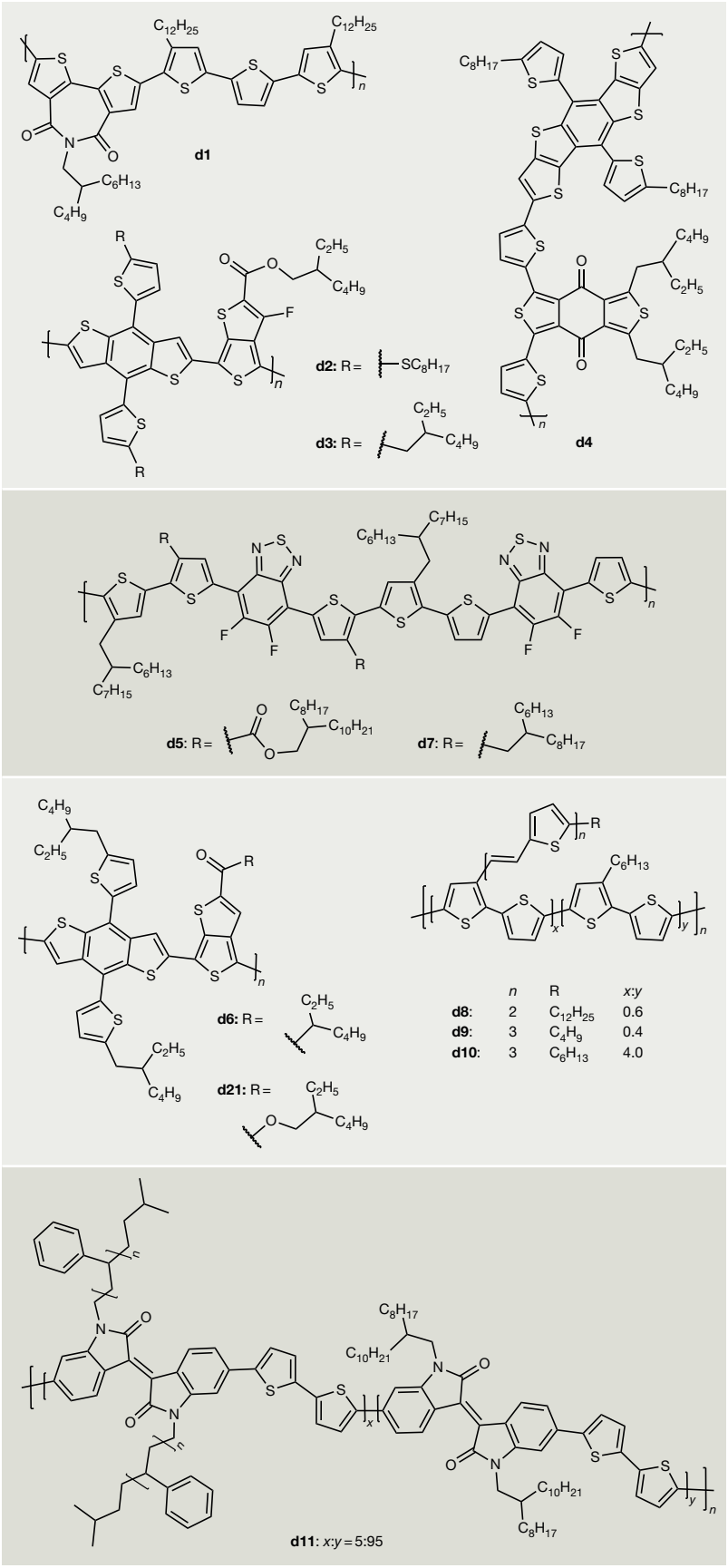

Figure 2 | **Representative polymeric electron donors (d1–d11, d21).** Chemical structures of selected electron-donor polymers.

smaller than $E_{b(D)}$ or $E_{b(A)}$). The V_{OC} is further reduced by radiative and non-radiative recombination processes (generally via the charge-transfer state). Thus, a compromise must be reached between the J_{SC}, which is maximized by absorbing as much visible and near-infrared (NIR) solar radiation as possible (for example, by using a material with broad absorption and low E_{op}), and the V_{OC}, which increases with an increase in $IE_{(D)} - EA_{(A)}$. For a single-junction cell that absorbs all photons with $E > E_{op}$ and none with $E < E_{op}$, the optimum E_{op} is ~1.1–1.4 eV (and PCE ≈ 34%) in the Shockley–Queisser limit[8]. The Shockley–Queisser limit assumes that no driving force is required for charge separation, enabling materials to be chosen such that $E_{op} = IE_{(D)} - EA_{(A)}$ and that there are no voltage losses from non-radiative recombination. In practice, however, a driving force is often needed for OSCs, and non-radiative recombination is unavoidable, leading to a higher optimum value of E_{op}. Increased deviation from these assumptions leads to increased energy losses:

$$E_{loss} = E_{op} - eV_{OC} \quad (7)$$

(or equivalently to increased voltage losses, E_{loss}/e), where e is the elementary charge. However, different considerations apply to tandem (and other multi-junction) cells; the highest-efficiency tandem cells consist of a large-E_{op} high-voltage sub-cell connected in series to a NIR-harvesting low-voltage sub-cell (with a lower E_{op} than the optimal value for a single-junction cell).

We note that the ionization-energy, electron-affinity and E_{op} values used in the preceding discussion are for solid films. E_{op} can be estimated from the long-wavelength onset of absorption, λ_{onset}, of a thin-film absorption spectrum ($E_{op} = 1240/\lambda_{onset}$, where λ_{onset} is in nm and E_{op} is in eV), although sometimes solution-based values are used, which may differ from the values for films, especially for molecules that strongly aggregate. However, ionization energy and electron affinity (often equated to $-E_{HOMO}$ and $-E_{LUMO}$, respectively, where E_{HOMO} is the energy of the HOMO (highest occupied molecular orbital) and E_{LUMO} is the energy of the LUMO) are usually estimated from electrochemical measurements, as the more direct techniques of measuring these values (UV photoelectron spectroscopy, for ionization energy, and particularly inverse photoelectron spectroscopy, for electron affinity) are much less widely available. Various relationships between redox potential and ionization energy or electron affinity have been proposed and used, but there is no reason to expect a universal and direct relationship because solvation energies (in electrochemistry) and solid-state polarization energies (affecting solid-state quantities), and the differences between them, depend on the size, shape and charge distribution of the relevant molecules and molecular ions[9]. Additional uncertainties in comparisons of electrochemically estimated ionization-energy and electron-affinity values arise from variations in potentials between solvents, from whether onset or half-wave potentials are used and from converting potentials between different reference couples. Thus, these values (including those discussed here) are only estimates; we emphasize that they should be compared with caution, especially in cases for which neither the original potentials nor the

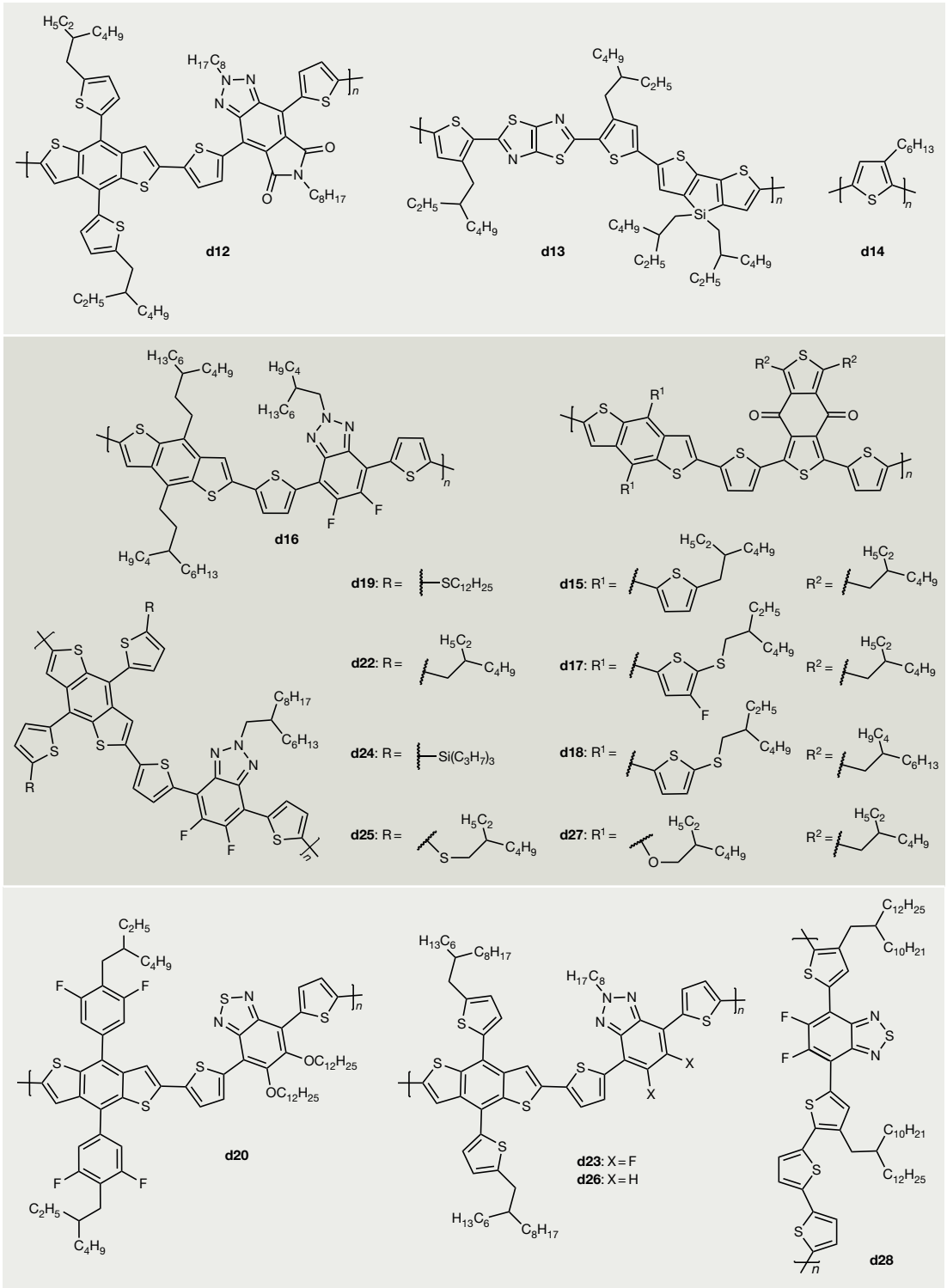

Figure 3 | **Representative polymeric electron donors (d12–d20, d22–d28).** Chemical structures of selected electron-donor polymers.

relationship used to obtain the ionization energy or electron affinity is specified. Furthermore, in some cases, the electron affinity is estimated from an electrochemical ionization energy or the ionization energy estimated from an electrochemical electron affinity, assuming IE – EA = E_{op}, thus neglecting E_b.

Fullerene versus non-fullerene acceptors

Although both effective donor and effective acceptor components are required for high-performance OSCs, the development of new donors (examples shown in FIGS. 2,3; note that all numbered donors are prefixed here with 'd' and acceptors with 'a') has received

more attention than that of new acceptors over the past decade.

Most OSCs have used FAs, particularly [6,6]-phenyl-C_{61}-butyric acid methyl ester ($PC_{61}BM$) and [6,6]-phenyl-C_{71}-butyric acid methyl ester ($PC_{71}BM$), despite some notable drawbacks (discussed below), and advances in donor materials have led to single-junction donor:FA BHJ OSCs with PCEs >11%[10–17]. Favourable qualities of FAs include their 3D character and delocalized LUMOs, which form extensive and robust charge percolation pathways; high electron mobilities (μ_e); electron-affinity values that are suitable for achieving charge separation with various donors (although, to some extent, this is because many donors have been designed for use with FAs); and the ability to form interpenetrating networks with donors, which is favourable for charge separation and charge transport.

Less desirable qualities of FAs include limited tunability of their electron affinities; weak absorption in the visible and NIR regions; thermal instability and photochemical instability[18]; limited utility in high-voltage sub-cells of tandem devices owing to their high electron affinities and low-lying singlet excited states[19]; and the need for time-consuming purification, which contributes to high costs, especially for more strongly absorbing C_{70} derivatives.

Organic NFAs offer the possibility of addressing these deficiencies of FAs: their chemical structures and electron affinities can be varied over a very wide range; they can exhibit increased visible–NIR absorptivity; and, at least in some cases, they can be more easily synthesized. On the downside, 2D planar conjugated organic building blocks tend to exhibit inherently anisotropic crystal structures and electron transport, which may complicate the formation of effective electron-extraction pathways. Moreover, the orientation of these planar molecules, which is difficult to control, affects several properties: the orientation with respect to the donor can in principle affect the energetics and dynamics of charge separation[20], the orientation with respect to the electrode can affect electron collection[21] and the relative orientation of adjacent anisotropic crystallites can affect electron transport. In addition, classical molecular dynamics simulations of amorphous molecular solids suggest that the percolation pathways for charges, which arise from the formation of networks of molecules linked through moderately strong intermolecular electronic couplings, are much more limited and fragile for 2D perylene diimide (PDI) NFAs than for $PC_{61}BM$ (REF. 22).

Ideally, NFAs should exhibit strong absorptions in regions of the visible and NIR spectrum that are complementary to those in which the available donors absorb; suitably matched energy levels for achieving charge separation with donors, with the minimal $-\Delta G_{CS}$ necessary (equation 2); the ability to form appropriate morphologies for charge separation; the ability to form percolation pathways for charge transport that support high μ_e in the morphologies formed in BHJ cells; and good molecular and morphological thermal stability and photostability.

NFAs have a long history; indeed, the first reported bilayer OSCs used a perylene-based acceptor[23], and some early BHJ OSCs used electron-rich and electron-poor poly(phenylene vinylene)s[24,25]. However, most BHJ work has used FAs, and only recently has the development of effective NFAs become a major focus of research[26–34]. Since 2015, concerted materials synthesis and device optimization efforts have increased PCEs for NFA OSCs from 6% to >13%[35,36], thus outperforming their fullerene counterparts (which have PCEs <13%)[17,37]. A wide variety of material classes have been examined as NFAs in BHJ OSCs, including (with the highest reported PCE values given in parentheses) rylene monoimides (5.44%)[38], tetracyanobutadiene derivatives (7.19%)[39], pentacene derivatives (1.29%)[40], twisted acene-imides (5.04%)[41], phthalocyanines (1.07%)[42], polymers containing B←N moieties (6.26%)[43] and numerous bis(acceptor)-terminated conjugated small molecules (for example, a bis(phthalimide vinyl)benzothiadiazole derivative, for which PCE = 3.7%)[19]. Other classes have been effective in planar heterojunction cells (for example, PCEs of up to 8.4% have been obtained for subphthalocyanines and subnaphthalocyanines)[44], but have not yet been examined in BHJ cells. However, many of the advances in NFA OSCs are attributable to two classes of materials: rylene diimides and fused-ring electron acceptors (FREAs), in which strongly electron-withdrawing end groups are attached to a fused-ring conjugated core bearing out-of-plane substituents. Accordingly, we focus our discussion on these two classes, both of which absorb strongly in the visible region and include examples that exhibit adequately high μ_e for achieving efficient OSCs. The electronic, optical and morphological characteristics of these two classes of materials can be extensively modulated through variation of the chemical structure, allowing for matching with various donor materials and leading to PCE values that, in some cases, rival or exceed those found for fullerene devices.

The device characteristics discussed in the following sections and summarized in TABLES 1–3 are generally those for the highest-PCE devices reported for each given donor–acceptor combination. However, note that device performance can depend on many other factors in addition to the nature of the donor and acceptor, including the donor:acceptor ratio, processing conditions (for example, the spin-coating rate and time, and the solvent and additives used), annealing conditions and device architecture (for example, whether the architecture is conventional or inverted, and the choice of electrode and interlayer materials).

Rylene diimides

Rylene diimides — that is, PDIs and naphthalene diimides (NDIs)[28,29,45,46] — along with related polyimide derivatives of other π-conjugated cores[41,47–49] are widely used as NFAs and exemplify both the advantages and drawbacks of NFAs. This class of NFA can exhibit electron affinities comparable with those of FAs; strong absorption; high μ_e in field-effect transistors, owing to intermolecular π stacking; and high thermal and oxidative stability[28,29,33,45]. Indeed, the first bilayer OSC used a perylene-based acceptor[23]. Transient absorption experiments on BHJ blends of simple monomeric PDIs with various polymeric

donors indicate efficient yields of charges, which were inferred from their long lifetimes to be well separated. Moreover, these yields are much more weakly dependent on $-\Delta G_{CS}$ than those for polymer:$PC_{61}BM$ blends[50,51]. However, BHJ OSCs using simple monomeric PDIs generally have low PCEs; for example, the PCE for a P3HT:*N,N′*-di(nonadecan-10-yl)-PDI blend[52] is only 0.18%. Many simple PDIs form 1D π stacks in their crystals; electron transport within a 1D π stack is much more efficient than electron transport between stacks. As noted, simulations of amorphous PDIs suggest more limited percolation pathways for charges than in $PC_{61}BM$ (REF. 22), with the 2D LUMOs of PDIs having an important role in determining these pathways. The observation of large crystalline PDI domains in some BHJs suggests that a lack of electron-transport pathways from these domains to the electrodes is a limitation in OSCs[50]. Furthermore, excitons in some 1D π-stacked PDI aggregates are rapidly deactivated by excimer formation[53]. However, despite these problems and the efforts dedicated to developing more complex molecular structures (see below), optimized BHJ OSCs consisting of certain molecular and polymeric donors in combination with the rather simple monomeric *N,N′*-di(pent-3-yl)-PDI have yielded PCEs ranging from 3% to 5%[54], with the highest value exceeding some reported using more complex PDIs (TABLE 1). Monomeric PDIs with 'ortho' (2, 5, 8 or 11) substituents (FIG. 4a) have been examined, having been predicated on the assumption that slip-stacked structures, in which the 'slip angle' between the π-stacking direction and the plane of the molecules is substantially less than 90°, can suppress excimer formation (by decreasing the intermolecular π–π interactions) while still providing intrastacked electron-transport pathways. Acceptor **a1** (FIG. 4b), the structure of which exhibits a slip angle of 47°, gave a PCE of 3.67% (TABLE 1) with donor **d1** (FIG. 2), and the relatively homogeneous morphology and small PDI domains likely contribute[55]. Nevertheless, most better-performing rylene diimide-based OSCs use more elaborate small-molecule or polymer structures, as described below.

Perylene diimide small molecules. As 1D π stacking in PDIs can have adverse effects, efforts have been made to suppress the formation of π stacks while trying to retain sufficient intermolecular LUMO–LUMO overlap for adequate electron transport. This can be achieved by constraining two or more PDIs to be non-coplanar and/or with the introduction of a conjugated bridging group. PDIs have been linked directly (such as in **a2**–**a6**, FIG. 4b), linked through a planar or non-planar core

Table 1 | **Optoelectronic properties and OSC device parameters for rylene diimide-based small-molecule electron acceptors (a1–a21)**

Acceptor	λ_{max} (nm)	E_{op} (eV)	EA/IE[a] (eV)	μ_e (10^{-5} cm^2 V^{-1} s^{-1})	Donor	V_{OC}[b] (V)	J_{SC}[b] (mA cm^{-2})	Fill factor[b] (%)	Highest PCE[b] (%)	Refs
a1	577	2.01	4.01/6.02	280[c]	**d1**	1.024	6.56	54.59	3.67	55
a2	–	2.04	3.86/5.90	41[d]	**d2**	0.80	12.85	53	5.58	63
a3	547	2.09	3.93/6.01	1.4[e]	**d2**	0.732	16.52	60.3	7.25	64
a4	–	2.07	4.04/6.13	3.32[e]	**d3**	0.80	11.98	59	5.90	66
a5	504	2.20	3.85/6.05	320[d]	**d4**	0.90	11.98	66.1	7.16	69
a6	474	2.22	3.87/6.09	640[d]	**d4**	0.96	12.49	70.2	8.42	70
a7	–	–	3.84/5.65	100[e]	**d6**	0.85	8.86	54.1	4.03	73
a8	–	–	3.62/5.99	–	**d5**	1.11	13.27	64.3	9.5	56
a9	–	1.76	3.70/5.40	3[d]	**d6**	0.88	11.92	33.6	3.32	74
a10	535	2.10	3.78/6.02	6.3[e]	**d3**	0.85	11.91	54.9	5.57	75
a11	530	2.05	3.81/6.03	27[e]	**d3**	0.78	17.10	68.5	9.15	75
a12	–	–	3.75/6.00	28[d]	**d7**	1.039	8.7	51	4.7	76
a13	–	–	3.72/5.77	100 ± 20[d]	**d7**	1.029	10.60	54	6.0	76
a14	500	2.10	3.76/5.86	230 ± 20[d]	**d7**	0.987	12.50	56	7.1	76
a15	575	–	3.89/5.71	0.61[e]	**d3**	0.79	17.9	58	8.47	77
a16	–	–	3.77/6.04	34[e]	**d3**	0.803	13.3	56.6	6.05	79
a17	–	–	3.86/6.23	15 ± 1[e]	**d3**	0.81	14.5	67	7.9	80
a18	–	–	3.91/6.26	1.5 ± 0.3[e]	**d3**	0.80	15.2	68	8.3	80
a19	474	2.22	3.77/5.98	16.3[e]	**d3**	0.94	12.48	58	6.72	81
a20	525	2.19	3.83/6.02	240[d]	**d4**	0.968	12.01	70.1	8.28	82
a21	530	2.17	3.80/5.97	320[d]	**d4**	1.00	12.99	71.5	9.28	82

λ_{max}, absorption maximum for film; μ_e, electron mobility; EA, electron affinity; E_{op}, the energy of the relaxed exciton relative to the ground state for the material with the lowest-energy absorption; IE, ionization energy; J_{SC}, short-circuit current density; OSC, organic solar cell; PCE, power conversion efficiency; V_{OC}, open-circuit voltage. [a]Measured or estimated using various techniques and with different assumptions; the values should be compared with caution and with reference to the original papers. [b]Different OSC studies use different donors, different donor:acceptor ratios, different processing conditions (including additives), and different electrodes and interfacial layers. Accordingly, values from different studies are often not directly comparable. [c]Measured in organic field-effect transistors. [d]Pristine film; μ_e measured by the space-charge-limited current (SCLC) method. [e]Blended film; μ_e measured by the SCLC method.

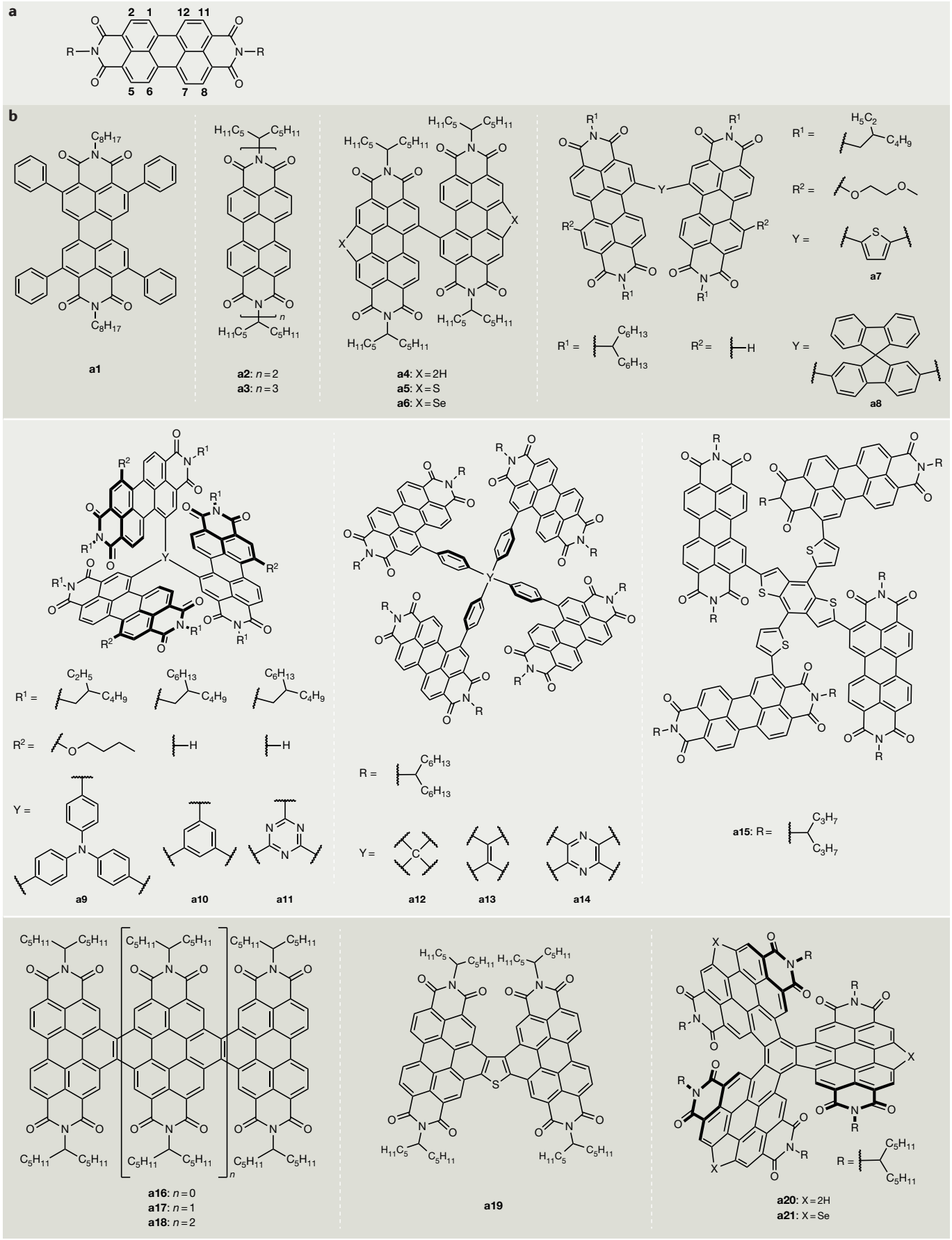

Figure 4 | **Rylene diimide-based small-molecule electron acceptors. a** | Atomic numbering of a perylene diimide structure. Positions 1, 6, 7 and 12 correspond to the 'bay' positions. Positions 2, 5, 8 and 11 correspond to the 'ortho' positions. **b** | Chemical structures of selected rylene diimide-based small-molecule electron acceptors (**a1**–**a21**).

(for example, **a7**–**a15**) and fused to one another (for example, **a16**–**a21**); linked or fused PDIs afford PCEs of up to 9.5%[56] (TABLE 1).

PDIs that are linked through a bond between the nitrogen atoms of the imide groups (for example, **a2** and **a3**) adopt an almost orthogonal orientation owing to steric and electrostatic repulsion between the imide oxygen atoms[57–64]. In a BHJ OSC, an analogue of **a2** exhibited a much higher PCE than a monomeric model (2.78% and 0.13%, respectively)[61]. The trimer **a3** slightly outperforms dimer **a2** in directly comparable OSCs with donor **d2** (5.81% and 5.58%, respectively); the much higher PCE of 7.25% for **a3**, given in TABLE 1, was obtained using an additive (diphenyl ether) to increase the domain purity in the active layer[64].

Dimers that are linked directly through a C–C bond also adopt twisted orientations; typically, the monomers are linked through the 'bay' (1,6,7 or 12) positions[65–70] (as in **a4**, FIG. 4b), although ortho examples are also known[71]. A dimer of a simple PDI (**a4**) with donor **d3** (widely known as PTB7-Th or PCE10) gave a PCE of 5.90%. Even higher PCEs can be achieved with the sulfur and selenium derivatives **a5** and **a6**, respectively, which have slightly lower electron affinities and absorb higher-energy photons than **a4**, with the absorption complementing that of donor **d4** (REFS 69,70) (TABLE 1).

Examples of dimers in which the bay positions of two PDI monomers are linked with an aromatic bridge include **a7** and **a8** (REFS 56,72,73). BHJ OSCs composed of acceptor **a8** and donor **d5** exhibit high PCEs, in part owing to a high V_{OC} of 1.11 V, and notably, the ultrafast and efficient formation of charges is observed despite a minimal $-\Delta G_{CS}$ (REF. 56; see section below on driving force and energy loss). Related molecules in which three or four PDIs are bound to a core, usually through their bay positions, have been extensively investigated (**a9**–**a15**)[74–78]. PDIs such as **a10** are necessarily non-coplanar owing to steric interactions between the PDI moieties. Others, such as **a12** (REF. 76) and an imide-nitrogen-linked analogue[78], use a 3D core and, in principle, could pack so as to facilitate isotropic electron transport. However, for both tri-PDI and tetra-PDI derivatives, species that are less dramatically distorted from planarity, such as **a11** (REF. 75) and **a14** (REF. 76), have yielded larger (but not excessively large) aggregates, higher μ_e and higher PCEs, suggesting that structures such as that of **a12** (REF. 76) go too far in disrupting the solid-state π stacking. The acceptor **a15** is a representative example in which the PDIs are linked to the core through their ortho positions[77]. PDIs that are linked through their ortho positions are typically more planar than their bay-linked counterparts, which facilitates closer packing of the π-conjugated backbone.

Fused oligomers **a16**–**a18** adopt helical structures owing to interactions between the ortho C–H groups of neighbouring PDIs[79,80]. For most of the oligomers discussed so far, the electrochemistry and spectra resemble those of monomeric PDIs. By contrast, **a16**–**a18** exhibit increasingly complex and redshifted spectra, and the electron affinity increases with increasing oligomer length, indicating substantial inter-PDI coupling. Despite the decreased μ_e in BHJ blends of longer oligomers with donor **d3**, **a18** forms network morphologies on appropriate length scales for achieving charge separation, which, together with its more effective light harvesting, results in an increased PCE. Relative to its thiophene-bridged PDI dimer precursor, **a19** exhibits reduced PDI–thiophene dihedral angles; has a lower electron affinity; and, in BHJ OSCs with **d3**, shows a 1,000-fold increase in μ_e and doubled PCE[81]. Single-crystal structures of propeller-like PDIs **a20** and **a21** show 3D networks of π interactions, which facilitate electron transport. Both **a20** and **a21** absorb over a much broader portion of the visible-light spectrum than simple PDIs and show a high PCE in BHJ blends with **d4** (REF. 82).

Rylene diimide polymers. All-polymer solar cells offer potential advantages, including long-term thermal and mechanical stability as well as superior control of solution viscosity, which is an important factor for the solution processing of large-scale OSCs[83,84]. However, non-ideal active-layer morphologies, especially low crystallinity and large domain sizes, often limit the PCE[85]. For example, donor **d14** with polymeric acceptor **a28** (FIG. 5) gave a PCE of only 0.2% owing to large-scale (~1 μm) phase segregation[86]. Conjugated polymers in which PDIs (linked through their bay positions) or NDIs (linked through their 2 and 6 positions) alternate with π bridges are among the best-performing polymer acceptors to date (FIG. 5; TABLE 2), affording PCE values in excess of 8%[87–89].

The first conjugated PDI polymers, **a22**–**a24**, used dithienothiophene (DTT) and DTT oligomers as the conjugated bridges[90–93]. As with many other polymers discussed here, these bridges are relatively electron rich. Accordingly, **a22**–**a24** have alternating donor and acceptor character, reminiscent of many polymers that have been developed for the donor role in OSCs, albeit with higher electron affinities and ionization energies. Because of the alternating donor–acceptor character, the onset absorptions are seen at much lower energies than those of typical PDIs (including many of those in TABLE 1); indeed, **a22**–**a24** absorb over much of the visible spectrum as a result of overlapping absorption bands that have DTT, PDI and charge-transfer character. OSCs with **d8** or **d9** as the donor and **a22**, **a23** or **a24** as the acceptor have yielded PCE values of 1.0–1.5%. A higher PCE of 3.45% was obtained for **a22** with donor **d6** in the presence of binary additives[94]; the PCE can be further increased (4.63%, TABLE 2) by the 'diluting concentrated solution' method, whereby an unusually concentrated polymer solution, enabling polymer entanglement, is diluted to a more typical concentration before spin coating[95]. Copolymers of PDIs with other fused-ring bridges, including carbazole (**a25**)[96–99], and with simple aromatic bridges, such as thiophene (**a26**)[100–102], have

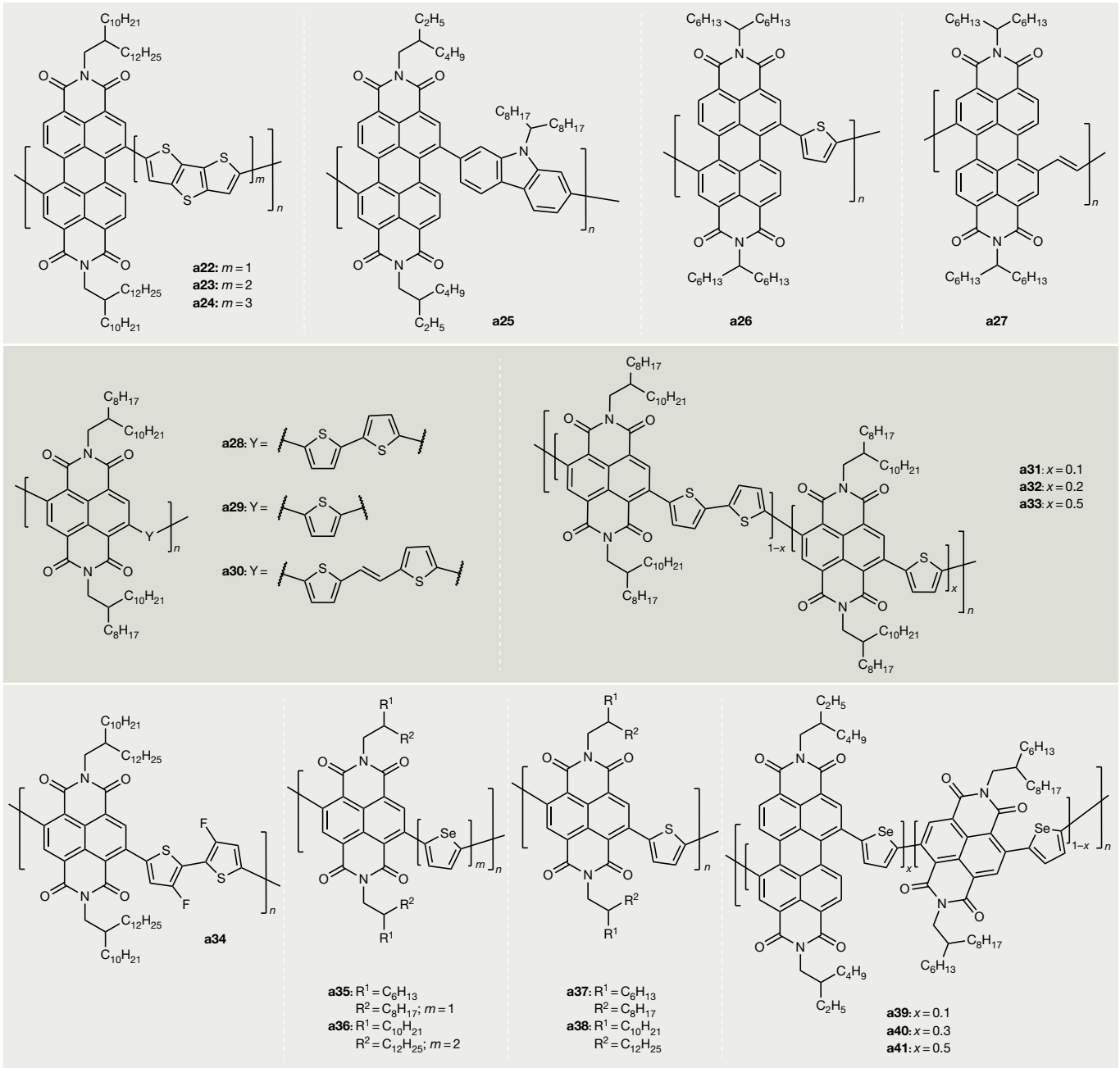

Figure 5 | **Rylene diimide-based polymeric electron acceptors.** Chemical structures of selected rylene diimide-based polymeric electron acceptors (**a22**–**a41**).

also been synthesized and examined in all-polymer solar cells. The vinylene linkers of **a27** improve the backbone planarity by reducing steric hindrance around the PDI bay region, which potentially improves π–π stacking and charge transport; indeed, **a27** exhibits a relatively high μ_e and a PCE of 7.57%[103]. Replacing the PDI unit of **a27** with a larger naphthodiperylenetetraimide unit leads to both increased absorption and reduced conformational disorder, contributing to a higher PCE of 8.59%[87].

Isolated NDIs have electron affinities comparable with those of PDIs and, although they absorb at higher energies than PDIs, the spectra of NDI polymers can be redshifted when combined with electron-rich linkers. Conjugated NDI polymers differ from their PDI analogues in that their backbones are more planar owing to less steric congestion. Moreover, as dibromo-NDI precursors are obtained as a single isomer (the 2,6-isomer), conjugated NDI polymers are obtained as regioregular rather than regiorandom structures, which may improve delocalization and π stacking. By contrast, dibromo-PDI precursors are obtained as a mixture of isomers (the 1,6-isomer and 1,7-isomer) that are not easily separated[104].

The NDI-bithiophene copolymer **a28** (widely known as N2200) exhibits a planar structure and dense packing, has a μ_e of 0.85 $cm^2 V^{-1} s^{-1}$ in field-effect transistors[105] and has been used in several OSC studies. OSCs based on

a28 and an imide-functionalized wide-bandgap polymer donor, **d12**, exhibit a PCE of 9.16%[89], which is the highest known value for all-polymer solar cells (see section below on donor–acceptor matching for further discussion). The polymers **a31**–**a33** randomly incorporate thiophenes in place of some bithiophenes, which reduces crystallinity and increases the achievable molecular weight relative to **a28**. As a result, among **a28** and **a31**–**a33**, **a31** exhibits the optimal miscibility with **d3** and the highest PCE of 5.6%, which can be improved further to 7.6% (TABLE 2) by solvent annealing[106].

Relative to **a28**, the difluorobithiophene analogue exhibits an increased PCE of 6.29% with **d3**, which is attributed to its increased crystallinity; further improvements are obtained using longer side chains on the NDI (6.71% for **a34**)[107]. The increased μ_e and PCEs seen for selenium-containing polymers, such as **a35** and **a36**, relative to their sulfur analogues have been attributed to improved intrachain interactions mediated by the selenium atoms[108–111].

Side-chain variation can greatly affect the OSC performance of NDI polymers, although these effects are not generalizable or well understood. For example, as noted, **a34** outperforms analogues with shorter side chains in BHJs with **d3**, but among blends of **a29**, **a37** and **a38** with **d3**, the polymer with the shortest chains yields the highest PCE[112–114].

NFA polymers incorporating both NDI and PDI monomers, **a39**–**a41** (REF. 115), have been synthesized. An increased PDI content leads to progressively smaller crystalline domains and larger π-stacking distances. Atomic force microscopy reveals that the phase-separation length scales in blends with donor **d6** are ~200, 100 and 20 nm for polymers **a35**, **a39** and **a40** with 0, 10 and 30 mol% PDI, respectively, whereas a clear contrast between **d6** and **a41** (50 mol% PDI) is not observed. Consistent with

Table 2 | **Optoelectronic properties and OSC device parameters for rylene diimide-based polymer electron acceptors (a22–a41)**

Acceptor	λ_{max} (nm)	E_{op} (eV)	EA/IE[a] (eV)	μ_e (10^{-5} cm^2 V^{-1} s^{-1})	Donor	V_{OC}[b] (V)	J_{SC}[b] (mA cm^{-2})	Fill factor[b] (%)	Highest PCE[b] (%)	Refs
a22	630	1.7	3.90/5.90	1,300[c]	**d8**	0.63	4.2	39	1.03	90
a22	–	–	–	–	**d6**	0.765	9.77	60.9	4.63	95
a23	647	1.5	3.80/5.70	–	**d9**	0.69	5.02	43	1.48	91
a24	678	1.5	4.00/5.40	70[c]	**d9**	0.69	2.80	40	0.77	92
a25	545	1.77	3.66/5.83	–	**d10**	0.70	6.35	50	2.23	98
a26	565	1.80	3.80/5.60	2[d]	**d11**	1.04	9.0	47	4.4	101
a27	598	1.74	4.03/5.77	150[e]	**d3**	0.74	15.9	63	7.57	103
a28	–	–	–	–	**d12**	0.844	15.48	70.10	9.16	89
a28	–	–	–	–	**d23**	0.83	14.18	70.24	8.27	88
a28	–	–	–	–	**d15**	0.87	11.7	57.5	5.8	159
a28	–	–	–	–	**d27**	0.82	6.8	43.0	2.4	159
a28	–	–	—	–	**d14**	0.52	1.41	29	0.21	86
a28	702	1.50	4.02/5.52	1.4[e]	**d3**	0.79	10.99	37	3.22	114
a29	600	1.70	3.94/5.64	0.65[e]	**d3**	0.80	8.85	43	3.03	114
a30	703	1.48	4.00/5.48	7[e]	**d3**	0.84	11.40	43	4.25	114
a31	694	1.55	4.05/6.36	60[d]	**d3**	0.83	12.9	71	7.6	106
a32	680	1.56	4.05/6.37	14[d]	**d3**	0.83	9.7	52	4.2	106
a33	644	1.60	4.00/6.38	9.5[d]	**d3**	0.83	5.8	48	2.3	106
a34	–	–	–	49[d]	**d3**	0.81	13.53	62	6.71	107
a35	614	1.65	4.00/5.65	10[d]	**d13**	0.76	7.78	55	3.26	108
a35	–	1.76	3.84/6.00	–	**d3**	0.81	18.80	51	7.73	110
a36	722	1.4	3.94/5.95	–	**d14**	0.53	3.79	44	0.88	111
a37	–	1.85	3.79/5.64	8.4[d]	**d3**	0.79	13.46	56	5.96	112
a38	–	1.83	3.81/5.64	0.13[d]	**d3**	0.81	7.81	52	3.25	112
a39	615	1.70	3.84/>5.95	85[d]	**d6**	0.78	6.94	51	2.8	115
a40	578	1.77	3.89/>5.95	100[d]	**d6**	0.79	18.55	45	6.29	115
a41	544	1.77	3.89/>5.95	18[d]	**d6**	0.73	9.68	38	2.66	115

λ_{max}, absorption maximum for film; μ_e, electron mobility; EA, electron affinity; E_{op}, the energy of the relaxed exciton relative to the ground state for the material with the lowest-energy absorption; IE, ionization energy; J_{SC}, short-circuit current density; OSC, organic solar cell; PCE, power conversion efficiency; V_{OC}, open-circuit voltage. [a]Measured or estimated using various techniques and with different assumptions; the values should be compared with caution and with reference to the original papers. [b]Different OSC studies use different donors, different donor:acceptor ratios, different processing conditions (including additives), and different electrodes and interfacial layers. Accordingly, values from different studies are often not directly comparable. [c]Measured in organic field-effect transistors. [d]Blended film; μ_e measured by the space-charge-limited current (SCLC) method. [e]Pristine film; μ_e measured by the SCLC method.

expectations regarding exciton diffusion lengths, **a40** with **d6** exhibits the highest peak external quantum efficiency (EQE) and PCE (5.1% under conditions comparable with those used for **a35** and **a39**; the higher value in TABLE 2 is obtained using an additional interfacial layer).

Fused-ring electron acceptors

FREAs consist of two strongly π-electron-withdrawing termini linked by a planar π bridge consisting of fused rings that are substituted with aryl or alkyl side chains that project above or below the plane[31]. Recently, considerable efforts have been made to improve FREA OSCs through variation of the fused-ring core, electron-withdrawing groups and side chains. Variation of the fused-ring core and electron-withdrawing groups can be used to tune the absorption wavelength, ionization energy and electron affinity. However, most examples discussed here (FIGS. 6,7; TABLE 3) have electron affinities fairly close to those of FAs and long-wavelength absorptions. Related molecules with cores that are more electron rich, weaker electron-withdrawing end groups and less sterically demanding core substituents have, however, been used as donors in OSCs[116]. For most of the BHJ OSCs in TABLE 3, the NFA is the lower-energy-absorbing component, whereas for most of the PDI small molecules in TABLE 1, the donor is the lower-energy absorber. The side chains affect solution processability, miscibility with donors and intermolecular packing. In particular, the presence of side chains suppresses the formation of 1D π stacks and π stacking in which the electron-rich core of one molecule interacts with the electron-poor end group of its neighbours. Thus, intermolecular π interactions are likely to occur primarily between the end groups, where the LUMO coefficients are highest, of considerably slipped neighbours. Indeed, molecular dynamics simulations suggest that films of **a46** (a FREA widely known as ITIC, FIG. 6) form robust 3D percolation networks based on such end-group-to-end-group π interactions and that these films are expected to exhibit higher and more isotropic electron transport than crystals of the same compound[117].

Effects of the core. A wide variety of NFAs have been developed in which two electron-withdrawing groups are linked through a conjugated core, including examples that can be regarded as FREAs owing to their small fused-ring cores, with out-of-plane substituents, such as 9,9′-dialkylfluorene[118,119], spirobifluorene[120] and dithienosilole[121] moieties. However, our focus here is on more recently developed FREAs with cores comprising five or more fused rings; the cores of such FREAs consist of dialkylcyclopentadiene or diarylcyclopentadiene rings fused with thiophene, selenophene and/or benzene (FIGS. 6,7). Indacenodithiophene (IDT) derivatives are among the most frequently used cores (examples include **a42**, **a51**–**a55** and **a68**–**a75**). FREAs with oligomeric IDT cores (**a43** and **a44**) have been compared with **a42**: larger cores decrease the ionization energy and redshift the absorption but lead to poorer π stacking, presumably owing to IDT–IDT twists and a decreased proportion of end groups relative to the core and side-chain moieties. The behaviour of this series of acceptors in OSCs is not straightforward to rationalize; **a42** forms poor-quality films with **d3** that give no photovoltaic response, but with **d4**, **a42** outperforms both **a43** and **a44** (REF. 122).

In general, larger fused-ring cores lead to more redshifted absorption and lower ionization energies, but direct comparison of **a42** (REF. 122) with **a45**–**a49** (REFS 123–127) in OSCs is not possible as not all of these acceptors have been tested with the same donor. Nonetheless, several examples with larger cores (including **a46** and **a47**) have exhibited PCEs >10%[123,128–132]. Replacing the central benzene ring of **a42** with thienothiophene affords **a45**; relative to **a42**, **a45** exhibits a greatly redshifted absorption and a μ_e that is one order of magnitude higher. Semi-transparent OSCs based on a blend of **d3** with **a45** exhibit a PCE of 9.77% with an average visible transmittance of 36%, outperforming all other reported single-junction and tandem semi-transparent OSCs[127]. An analogue of **a49** in which the outer thiophene rings are replaced by selenophene (**a50**) has similar optical and electrochemical properties to those of **a49** but has a higher μ_e (REF. 133). The OSC performances of **a49** and **a50** have not been directly compared as these acceptors do not use the same donor.

Effects of the end group. The choice of end group also affects the optical and electrochemical properties of FREAs (TABLE 3). Many FREAs incorporate the 1,1-dicyanomethylene-3-indanone end group[134]. However, compounds **a51**–**a53**, for example, have benzothiadiazole–rhodanine end groups, have smaller estimated electron affinities than their 1,1-dicyanomethylene-3-indanone analogue (**a42**) and, in the corresponding OSCs incorporating the same donors, exhibit higher V_{OC} values[135–139]. Compound **a55** can be regarded as both an example of a bis(PDI)-core (related to **a7** and **a8**) and as a FREA[140]. Density functional theory calculations suggest that **a55** has a much less planar π system than that of other FREAs, presumably resulting in relatively weak core–acceptor coupling. Moreover, its reduction potential is typical for PDIs (and is close to that of $PC_{61}BM$ and **a42**), and its absorption spectrum shows a PDI-like peak in addition to a low-energy charge-transfer band. Thus, in many respects, **a55** is more PDI-like than FREA-like.

Variations have been made on the 1,1-dicyanomethylene-3-indanone end groups of compounds **a42**–**a50**. Mono-methylation and di-methylation of the end groups of **a46** (widely known as ITIC) to give **a56** and **a57**, respectively, lead to slightly blueshifted absorptions and slightly smaller electron affinities, resulting in slight increases in the V_{OC} of OSCs with **d15** (note that the electron affinity of **a46** was estimated to be 4.02 eV in a direct comparison with **a56** and **a57** and is larger than the value in TABLE 3). The highest PCE values, however, were found for **a56**; this was attributed to higher phase purity and more ordered donor aggregates[141]. In contrast to methylation, partial fluorination of the end groups leads to redshifted absorption, increased electron affinity and increased μ_e, as seen for **a48** when compared with **a58**–**a60**. In OSC blends with **d16**, the V_{OC} decreases with the extent of fluorination, consistent with the electron-affinity values, but this is more than offset by the increased J_{SC} (REF. 125). When the donor and acceptor

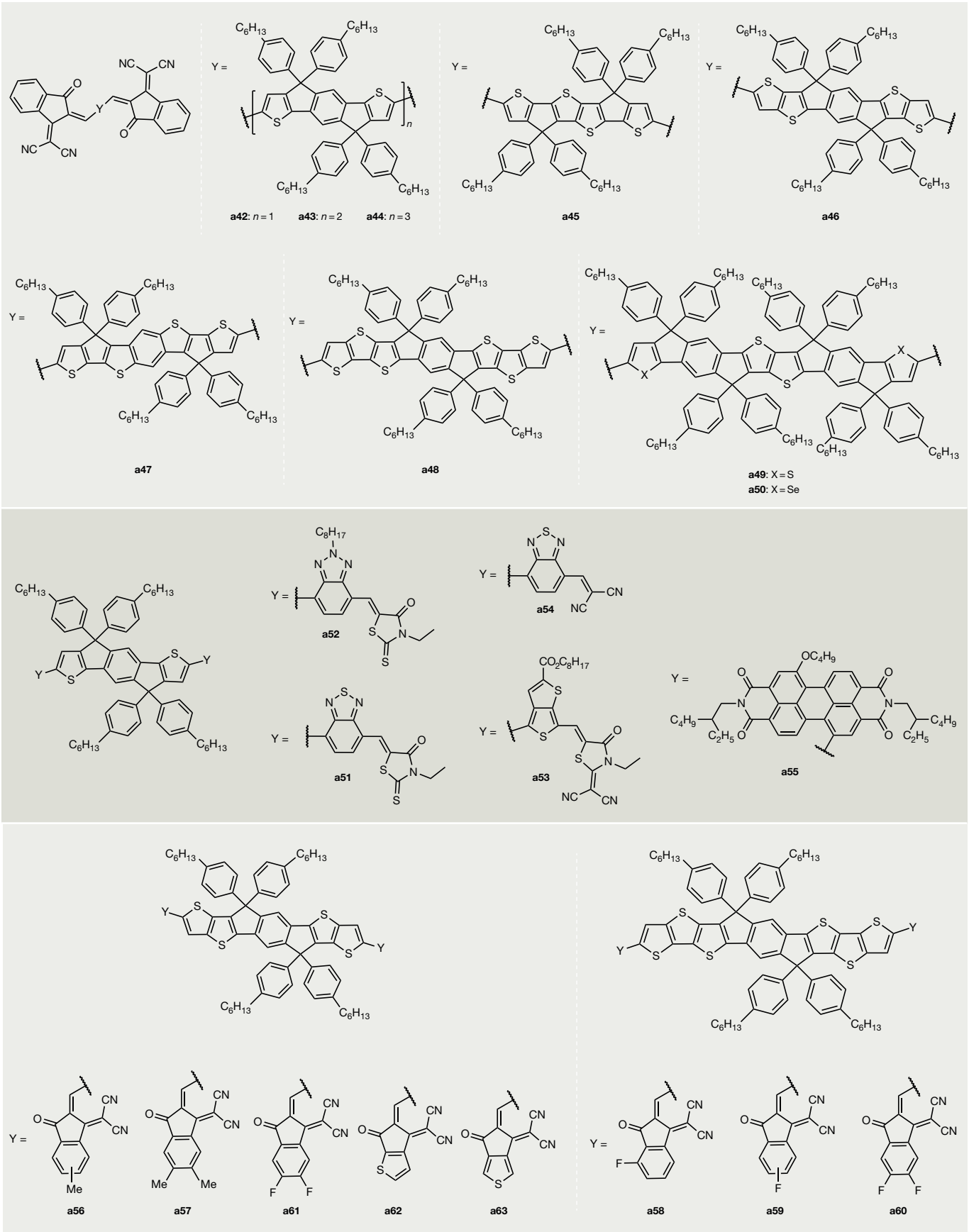

Figure 6 | **Fused-ring electron acceptors (a42–a63).** Chemical structures of selected fused-ring electron acceptors.

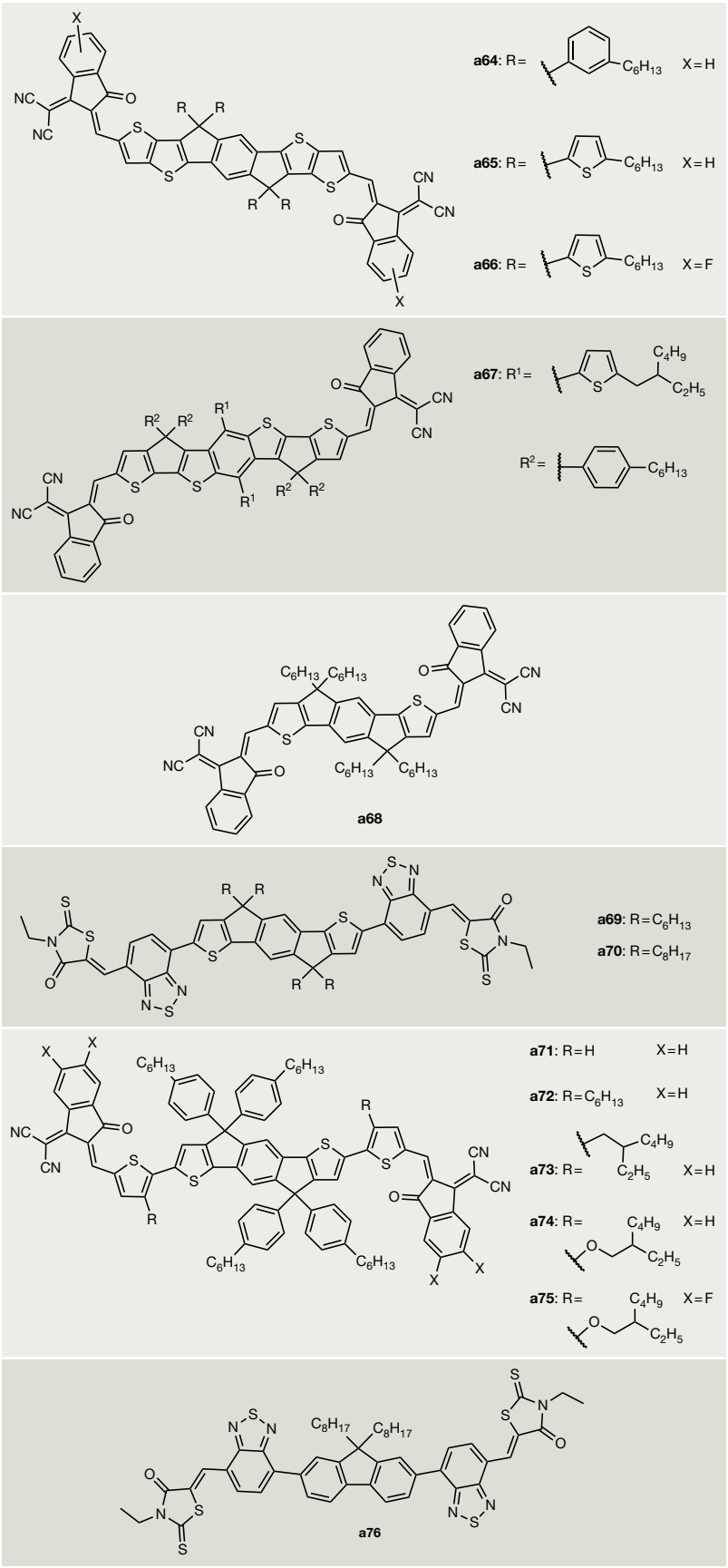

Figure 7 | **Fused-ring electron acceptors (a64–a76).** Chemical structures of selected fused-ring electron acceptors.

are both fluorinated there is less of a decrease in the V_{OC}, and the OSCs based on the **d17**:**a61** blend yield a high J_{SC} value of 20.50 mA cm^{-2} and a PCE of 13.1%, which is the highest value for a single-junction OSC[35].

The 1,1-dicyanomethylene-3-indanone end group can also be modified by replacing benzene with thiophene[142,143] or naphthalene[144]. For example, introduction of a thiophene ring slightly affects electronic properties and enhances intermolecular interactions, crystallinity and μ_e, leading to a higher fill factor and higher PCE, as seen for **a62** and **a63** compared with **a46** (REFS 142,143). The introduction of naphthalene has similar effects[144].

Effects of the side chain. Although aryl or alkyl side chains can have minor effects on the electronic properties, they have a more notable effect on intermolecular interactions, both between adjacent FREA molecules and between FREA molecules and donor materials. Therefore, side chains can be used to tailor solubility, crystallinity, μ_e and active-layer morphology. As also seen for some of the rylene diimides, even subtle variations in the side chains can have a great influence on the OSC performance. For example, **a64** is an isomer of **a46**, differing only in *meta*-hexylphenyl rather than *para*-hexylphenyl substituents, but forms more crystalline films with a greater proportion of acceptors adopting a 'face-on' orientation. It also exhibits a higher μ_e and, in OSC blends with **d19**, demonstrates higher PCEs[130] (TABLE 3). Replacement of the hexylphenyl side chains of **a46** with inductively electron-withdrawing 5-hexyl-2-thienyl groups (**a65**) leads to a slight increase in the ionization energy and electron affinity, as well as a higher μ_e (REFS 124,145). FREA **a66** combines 5-hexyl-2-thienyl side chains with partially fluorinated termini, which redshift the absorption and further increase the electron affinity and μ_e. As a result, OSCs based on **d16**:**a66** exhibit higher PCEs than those of **d16**:**a65** (REF. 146). Relative to **a47**, **a67**, with conjugated alkyl-2-thienyl side chains on the central benzene ring, exhibits redshifted and stronger absorption, slightly smaller electron affinity and ionization energy and higher μ_e. OSCs based on **d16**:**a67** blends have a much higher PCE of 11.0% than that of **d16**:**a47** (8.54%)[147].

Compared with aryl substituents, flexible alkyl substituents can adopt conformations that do not project as far above or below the plane of the core, enabling increased intermolecular π overlap. Replacement of the aryl groups of **a42** with *n*-hexyl chains to afford **a68** (REF. 148) leads to a redshift in the solid-state absorption and to an increase in μ_e. OSCs based on **d4**:**a68** exhibit higher PCEs than those based on **d4**:**a42** (REF. 122); the PCE can be further increased by using different donors, notably **d20** (REF. 149). Acceptors **a69** (REF. 139) and **a70** (REF. 150) also exhibit film spectra that are redshifted from that of the aryl analogue **a51** (REF. 135) and outperform **a51** in directly comparable OSCs with **d3** and **d14** (widely known as P3HT), respectively (note that the higher PCE in TABLE 3 for **d3**:**a51** is for a cell containing an additional acceptor[136] and that **d14**:**a70** cells with a PCE of 7.7% are obtained by the addition of another FREA[151]). FREAs **a71**–**a74** differ in the side chains

Table 3 | **Optoelectronic properties and OSC device parameters for fused-ring electron acceptors (a42–a75)**

Acceptor	λ_{max} (nm)	E_{op} (eV)	EA/IE[a] (eV)	μ_e (10^{-5} cm^2 V^{-1} s^{-1})	Donor	V_{OC}[b] (V)	J_{SC}[b] (mA cm^{-2})	Fill factor[b] (%)	Highest PCE[b] (%)	Refs
a42	688	1.70	3.83/5.91	45[c]	**d4**	0.92	13.39	60.0	7.39	122
a43	692	1.57	3.80/5.42	8.4[c]	**d3**	0.93	12.75	37	4.38	122
a44	704	1.53	3.79/5.29	12[c]	**d3**	0.93	3.51	32	1.05	122
a45	796	1.38	3.93/5.45	240[c]	**d3**	0.754	19.01	68.1	9.77[d]	127
a46	702	1.59	3.83/5.48	30[c]	**d3**	0.81	14.21	59.1	6.80	124
a46	–	–	–	–	**d24**	0.94	17.32	69.77	11.41	129
a46	–	–	–	–	**d15**	0.899	16.81	74.2	11.21	128
a46	–	–	–	–	**d19**	0.898	17.97	65.49	10.57	130
a46	–	–	–	–	**d23**	0.82	16.47	69	9.26	157
a46	–	–	–	–	**d25**	0.91	16.33	60.38	8.97	158
a46	–	–	–	–	**d22**	0.73	13.11	57.80	5.51	158
a46	–	–	–	–	**d26**	0.71	12.93	53	4.80	157
a47	731	1.56	3.83/5.40	13.8[e]	**d15**	0.868	17.85	67.2	10.42	123
a48	706	1.57	3.88/5.45	6.1[c]	**d16**	0.957	13.51	57.9	7.7	125
a49	721	1.53	3.82/5.42	4.54[e]	**d3**	0.94	14.49	47.5	6.48	126
a50	–	1.52	3.81/5.41	1.27[c]	**d23**	0.91	15.16	58	8.02	133
a51	658	1.68	3.69/5.52	34[c]	**d14**	0.84	8.91	68.1	5.12	135
a51	–	–	–	–	**d3**	1.03	14.5	65.0	10.1	136
a52	–	1.85	3.55/5.51	–	**d14**	1.02	7.34	70	5.24	137
a53	736	1.54	3.63/5.50	24[e]	**d3**	0.87	16.48	70	10.07	138
a54	688	1.60	3.8/5.6	1.0[e]	**d6**	0.766	10.10	55.1	4.26	177
a55	–	1.54	3.83/5.53	39[e]	**d14**	0.70	5.58	66.8	2.61	140
a56	700	1.60	3.98/5.58	11[e]	**d15**	0.94	17.44	73.5	12.05	141
a57	692	1.63	3.93/5.56	4.7[e]	**d15**	0.97	16.48	70.6	11.29	141

attached to the thiophene bridges between the fused-ring core and the terminal groups. In OSCs with donor **d3**, the derivative with linear alkyl chains, **a72**, has a higher domain purity, μ_e and PCE than **a71** (which does not have a substituent on the bridge) and **a73** (which has a branched alkyl chain)[152–154]. The alkoxy-substituent of **a74** leads to a redshifted absorption, decreased ionization energy and increased electron affinity; **d21:a74** OSCs exhibit higher PCEs than **d21:a73** devices (4.9%)[155]. Subsequently, a record-high PCE of 13.8% was obtained for **d21:a74**-based tandem devices[36]. Compared with **a74**, FREA **a75**, which has difluorinated termini, exhibits redshifted absorption and a narrower bandgap. An OSC based on a binary blend of **d3** with **a75** has a PCE of 10.0%, whereas an OSC based on a **d3:d22:a75** ternary blend exhibits an even higher PCE of 10.9%, with a higher J_{SC} of 25.3 mA cm^{-2} (REF. 156).

Device considerations

In addition to the development of NFAs, full realization of their potential will require an understanding of how to optimally combine them with donor materials and knowledge of the photophysical and electrical properties of these blends. Below, we briefly survey several device-relevant aspects of NFAs.

Donor–acceptor matching. The tunable electronic and optical properties of NFAs widen the choice of donors from which high-performance OSCs can be constructed. In general, donors should have energy levels (such as ionization energy, electron affinity and E_{op}) that are sufficient for engendering efficient charge separation, but which minimize E_{loss} (see section below on driving force and energy loss); absorb light of complementary wavelengths to those absorbed by the NFA to maximize light harvesting and the J_{SC}; have high hole mobility (μ_h), comparable to the NFA μ_e, to help achieve high J_{SC} and high fill factors; and exhibit phase separation on an appropriate scale and with appropriate molecular orientation to facilitate efficient charge separation and charge percolation pathways.

Some of these properties, such as the energetic quantities, can be rationally selected and/or controlled; others, such as those relating to blend morphology, are more difficult to predict. In addition, some of these properties are interrelated; for example, μ_h is often strongly dependent on the morphology. Thus, donor choice is still, at least partly, based on trial and error. For example, acceptor **a46** yields PCEs that vary from 5% to more than 11% when paired with a series of related polymers — donors **d19** and **d22**–**d26** (TABLE 3) — all of which show similar absorption spectra that complement that of the NFA[129,130,157,158].

Table 3 (cont.) | **Optoelectronic properties and OSC device parameters for fused-ring electron acceptors (a42–a75)**

Acceptor	λ_{max} (nm)	E_{op} (eV)	EA/IE[a] (eV)	μ_e (10^{-5} cm^2 V^{-1} s^{-1})	Donor	V_{OC}[b] (V)	J_{SC}[b] (mA cm^{-2})	Fill factor[b] (%)	Highest PCE[b] (%)	Refs
a58	720	1.56	3.97/5.54	10[c]	**d16**	0.929	16.63	64.3	10.1	125
a59	728	1.52	3.98/5.52	12[c]	**d16**	0.903	17.56	66.8	10.8	125
a60	744	1.48	4.02/5.52	17[c]	**d16**	0.852	19.68	68.5	11.5	125
a61	717	–	4.14/5.66	50.5[c]	**d17**	0.88	20.88	71.3	13.10	35
a62	670	1.67	3.76/5.47	92.6[c]	**d15**	1.01	15.9	71	11.4	142
a63	720	1.58	3.96/5.62	320[c]	**d18**	0.95	16.5	75.1	11.8	143
a64	700	1.58	3.82/5.52	24.5[c]	**d19**	0.912	18.31	70.55	11.77	130
a65	706	1.60	3.93/5.66	61[c]	**d4**	0.88	16.24	67.1	9.6	145
a66	728	1.55	4.01/5.74	760[e]	**d16**	0.849	19.33	73.73	12.1	146
a67	738	1.53	3.80/5.43	130[c]	**d16**	0.925	18.88	63.0	11.0	147
a68	716	1.62	3.91/5.69	110[c]	**d4**	0.85	15.85	68.0	9.20	149
a68	–	–	–	–	**d20**	0.905	17.30	70.8	11.03	149
a69	690	1.61	3.67/5.37	220[c]	**d3**	0.95	15.2	60.0	8.7	139
a70	690	1.63	3.88/5.51	0.3–0.6[e]	**d14**	0.72	13.9	60	6.4	150
a71	712	1.62	3.87/5.44	20[e]	**d3**	0.84	9.9	44	3.9	154
a72	726	1.60	3.86/5.46	600[e]	**d3**	0.93	12.8	58	7.4	154
a73	716	1.61	3.85/5.48	25[e]	**d3**	0.95	12.3	49	6.0	154
a74	805	1.34	3.95/5.32	14[c]	**d21**	0.82	17.7	58	8.4	155
a75	–	1.24	4.19/5.44	11.4[c]	**d3**	0.739	22.8	59.4	10.0	156

λ_{max}, absorption maximum for film; μ_e, electron mobility; EA, electron affinity; E_{op}, the energy of the relaxed exciton relative to the ground state for the material with the lowest-energy absorption; IE, ionization energy; J_{SC}, short-circuit current density; OSC, organic solar cell; PCE, power conversion efficiency; V_{OC}, open-circuit voltage. [a]Measured or estimated using various techniques and with different assumptions; the values should be compared with caution and with reference to the original papers. [b]Different OSC studies use different donors, different donor:acceptor ratios, different processing conditions (including additives), and different electrodes and interfacial layers. Accordingly, values from different studies are often not directly comparable. [c]Pristine film; μ_e measured by the space-charge-limited current (SCLC) method. [d]Performance of semi-transparent OSC devices. [e]Blended film; μ_e measured by the SCLC method.

Some of these OSC parameters can be rationalized based on the polymer properties; for example, V_{OC} values correlate well with the ionization energy of the polymer (which varies from 5.13 eV for **d26** to 5.40 eV for **d24**).

Studies of OSCs in which polymer **a28** is combined with various donors illustrate the importance of the morphology[86,89,159]. Each of the donor polymers **d14**, **d15**, **d27** and **d12** absorbs a portion of the visible-light spectrum that is more or less complementary to that absorbed by the acceptor polymer, and each is anticipated to exhibit $\Delta G_{CS} < 0$; however, as shown in TABLE 2, the PCEs vary enormously. The very low PCE obtained with **d14** was attributed to the hierarchy of phase separation (X-ray microscopy reveals coarse phase separation with domain sizes of 0.2–1 μm, whereas the photoluminescence of **d14** is still efficiently quenched, indicating intermixing within these mesoscale domains), presumably leading to both ineffective exciton dissociation and rapid geminate recombination[86]. Differences between blends with **d15** and **d27** were attributed to higher crystallinity in the latter, coupled with a different molecular alignment relative to both the donor–acceptor interface and the electrodes, leading to more efficient hole transport and more efficient dissociation of the donor–acceptor charge-transfer states[159]. Blends of **a28**:**d12** afford the highest PCE of 9.16% as a result of a homogeneous morphology with finely divided domains[89].

Two specific aspects of OSC performance that are dependent on the combination of donor and acceptor — the driving force for charge separation and the fill factor — are discussed in more detail below.

Driving force and energy loss. To increase the PCE towards the Shockley–Queisser limit, it is necessary to minimize the energy loss, E_{loss} (equation 7). One contributor to E_{loss} is $E_{op} - E_{CT}$ (where the E_{op} is for the lowest-energy absorber); other contributions are associated with radiative and non-radiative decay (see REF. 160 for an alternative breakdown of the contributions to E_{loss}). $E_{op} - E_{CT}$ can be rewritten (using equations 6 and 2) as $E_{op} - IE_{(D)} + EA_{(A)} + E_{b(CT)}$ and so is closely related to $-\Delta G_{CS}$, differing in the contributions of $E_{b(CT)}$ and $T\Delta S_{CS}$, respectively. Historically, it was considered that $EA_{(A)} - EA_{(D)}$ and $IE_{(A)} - IE_{(D)}$ should be ≥0.3 eV to provide sufficient $-\Delta G_{CS}$ to achieve appreciable photocurrent[161,162]. As a consequence of the related offset between E_{op} and E_{CT}, and also to charge-transfer state decay processes, the lower limit for E_{loss} in OSCs was thought to be 0.6 eV (REF. 163), and generally, the most efficient OSCs suffer from high E_{loss} values.

However, OSCs have been reported in which efficient photocurrent generation is observed despite vanishing $-\Delta G_{CS}$, which can be inferred from electrochemical estimates of $EA_{(A)} - EA_{(D)}$ from equation 2 (using electrochemical and optical data and ignoring the entropic term) and/or from $E_{op} - E_{CT}$ (using highly sensitive EQE measurements and/or electroluminescence measurements). Both FA[164–167] and NFA[56,136,168] examples have now been reported in which small $-\Delta G_{CS}$ and $E_{loss} \leq 0.6$ eV are observed. For example, **d5:a8** (TABLE 1) exhibits $E_{CT} \sim E_{op(D)}$ and $E_{loss} = 0.61$ eV, and yet exciton dissociation occurs on a 3 ps timescale, and the PCE is a very respectable 9.5%[56]. For **d28:a76** (FIGS. 3,7), equation 2 suggests that $\Delta G_{CS} \approx 0$ if the entropic contribution is neglected; the EA offset is estimated to be 0.05 eV, $E_{loss} = 0.5$ eV, the excitons dissociate with a lifetime of ~48 ps and the PCE is 7.8% (the same polymer has a much higher E_{loss} of 0.85 eV with $PC_{71}BM$, owing to both a lower E_{CT} and increased non-radiative decay)[168]. Both of these OSCs also exhibit high V_{OC} values of ~1.1 V. As well as the small $-\Delta G_{CS}$ that is evidently required, the non-radiative contributions to E_{loss} are calculated to be small (0.23–0.26 eV) and are comparable with the best values obtained for FA cells, for which the non-radiative losses follow an energy-gap law, being lowest for the highest E_{CT} cells[169].

Although the usually neglected entropic contribution to $-\Delta G_{CS}$ may play a part, it is not yet clear why some systems (including both FAs and NFAs) exhibit efficient charge separation with such small values of $E_{op} - E_{CT}$ and/or small EA offsets, whereas many others do not. However, the emergence of many high-performance donors and NFAs potentially enables fine-tuning of these energy offsets and thus a more thorough study of the interrelation of $-\Delta G_{CS}$, $E_{op} - E_{CT}$, charge separation and charge recombination losses, which would enable us to more fully understand how to simultaneously maximize both J_{SC} and V_{OC}. Moreover, although some non-radiative recombination is inevitable in OSCs, a more thorough understanding of the relevant vibrational modes that deactivate excited charge-transfer states, coupled with careful design of NFAs and of donors, might lead to a further decrease in the associated losses.

Fill factor. Besides J_{SC} and V_{OC}, it is also important to maximize the fill factor of NFA OSCs. The fill factor is related to the competition between the recombination and extraction of free charges[170] and depends on a μ_h and μ_e for the donor–acceptor blend and the thickness of the active layer. For active layers that are ~100 nm thick, μ_h and μ_e of $\sim 10^{-4}$–10^{-3} $cm^2 V^{-1} s^{-1}$ can be sufficient to achieve fill factors of more than 70%, whereas for thicker films that absorb more light, higher mobilities are needed to achieve the same fill factor (for example, $\sim 10^{-2}$ $cm^2 V^{-1} s^{-1}$ for 300 nm films). Meanwhile, it is also important to obtain sufficiently pure donor and acceptor domains to achieve high fill factors for thick-film OSCs[171–174]. FA μ_e values ($\sim 10^{-3}$–10^{-2} $cm^2 V^{-1} s^{-1}$) allow for high fill factors in thick devices. However, few NFAs show μ_e of this magnitude, at least in BHJ blends (TABLES 1–3); thus, the highest-PCE devices and those that display high fill factors are generally ~100 nm in thickness. Therefore, there remains a need to develop NFAs with μ_e near or higher than those of fullerenes, as well as to learn how to achieve sufficiently pure, yet appropriately sized, donor and NFA domains in BHJ blends.

Conclusion and future perspectives

Rapid advances have recently been made in the development of NFAs for inclusion as the active layer of BHJ OSCs, with rylene diimides and FREAs providing the most promising results. Generally, compared with PDI small molecules, the FREAs examined to date exhibit similar electron affinities and mobilities, but considerably redshifted absorption with higher absorptivities. Consequently, to realize complementary absorption, FREAs are more suitable for pairing with wide-bandgap donors, whereas perylene diimide small molecules are suitable for pairing with narrow-bandgap donors. As wide-bandgap donors usually exhibit higher ionization energies than their narrow-bandgap counterparts, high V_{OC} and high J_{SC} can be achieved simultaneously for OSCs based on blends of wide-bandgap donors with FREAs. As well as applications in the active layer, NFAs can also function as electron-extracting electrode interlayer materials in OSCs; for example, a PDI material has recently been shown to increase the V_{OC}, J_{SC} and fill factor for inverted polymer donor:FA BHJ cells, leading to large increases in PCE[175].

Owing to concerted efforts in material synthesis, morphology control and device optimization, the PCEs of FREA OSCs have now exceeded 13%, which is higher than that of the best-performing FA OSCs and approaching the 15% target that is generally considered necessary for commercial application. However, several challenges remain in order to further increase the PCE of NFA OSCs. As noted (see section on driving force and energy loss), recent studies indicate that the driving forces needed to achieve efficient charge separation can be much lower than previously thought, which in some cases lead to lower values of E_{loss}. However, a detailed understanding of why only certain systems function in this way is still lacking, and questions remain as to whether such low E_{loss} values can be combined with the highest J_{SC} and fill factor values to afford record-high PCEs. It is also unclear why low non-radiative recombination rates, which help in achieving low E_{loss}, are found for some systems, and the extent to which these can be more generally achieved and/or further reduced to minimize E_{loss} in a more rational way. Another apparent limitation is the difficulty in achieving high μ_e to improve the fill factors of thicker NFA OSCs to compete with those for FA OSCs. All these issues require a more thorough understanding of the roles of the chemical structures and energetic characteristics of both the donor and acceptor on morphological, photophysical and charge-transport properties of BHJ blends than is currently available.

Acceptors with strong NIR absorption[127,131] or with a high electron affinity will enable the use of NIR-absorbing donor polymers for fabricating semi-transparent, ternary-blend and tandem devices. Although NFAs are much better suited for such challenges and opportunities

than FAs, owing to their more easily tunable chemical and electronic structures and stronger light absorption, this area largely remains unexplored. Appropriately designed NFAs can also help facilitate high-V_{OC}, short-wavelength absorbing sub-cells for use in tandem devices, a role for which FAs are intrinsically unsuitable owing to their relatively low excited-state energies.

Commercialization will also require simple device fabrication methods that do not sacrifice performance. In this regard, the solution processability of OSCs compared with many other photovoltaic technologies is a strong point. However, most of the high-PCE devices reported in TABLES 1–3 have been achieved using spin coating, a process in which ~90% of the active material may be wasted and is thus unsuitable for large-area devices. Therefore, a more material-efficient method for OSC fabrication, such as roll-to-roll printing or doctor blading, is needed. The OSC community needs to better understand how to successfully retain the performance of spin-coated OSCs in cells processed by these other methods. Long-term stability is another key requirement for the commercial deployment of OSCs. Although some studies report better stability for NFA-based OSCs than for their FA-based counterparts[151,176], more efforts are required to systematically elucidate molecular and morphological stability to oxygen, moisture, heat, irradiation and mechanical stress, in addition to the associated mechanisms of device failure.

1. Cheng, Y., Yang, S. & Hsu, C. Synthesis of conjugated polymers for organic solar cell applications. *Chem. Rev.* **109**, 5868–5923 (2009).
2. Li, G., Zhu, R. & Yang, Y. Polymer solar cells. *Nat. Photonics* **6**, 153–161 (2012).
3. Krebs, F. C., Espinosa, N., Hosel, M., Sondergaard, R. R. & Jorgensen, M. 25th anniversary article: rise to power — OPV-based solar parks. *Adv. Mater.* **26**, 29–38 (2014).
4. Darling, S. B. & You, F. The case for organic photovoltaics. *RSC Adv.* **3**, 17633–17648 (2013).
5. Deibel, C. et al. Energetics of excited states in the conjugated polymer poly(3-hexylthiophene). *Phys. Rev. B* **81**, 085202 (2010).
6. Yu, G., Gao, J., Hummelen, J. C., Wudl, F. & Heeger, A. J. Polymer photovoltaic cells - enhanced efficiencies via a network of internal donor-acceptor heterojunctions. *Science* **270**, 1789–1791 (1995).
7. Vandewal, K., Tvingstedt, K., Gadisa, A., Inganas, O. & Manca, J. V. On the origin of the open-circuit voltage of polymer–fullerene solar cells. *Nat. Mater.* **8**, 904–909 (2009).
8. Shockley, W. & Queisser, H. J. Detailed balance limit of efficiency of *p-n* junction solar cells. *J. Appl. Phys.* **32**, 510–519 (1961).
9. Sworakowski, J., Lipinski, J. & Janus, K. On the reliability of determination of energies of HOMO and LUMO levels in organic semiconductors from electrochemical measurements. A simple picture based on the electrostatic model. *Org. Electron.* **33**, 300–310 (2016).
10. Chen, H. et al. Polymer solar cells with enhanced open-circuit voltage and efficiency. *Nat. Photonics* **3**, 649–653 (2009).
11. Liang, Y. et al. Development of new semiconducting polymers for high performance solar cells. *J. Am. Chem. Soc.* **131**, 56–57 (2009).
12. Liang, Y. & Yu, L. A new class of semiconducting polymers for bulk heterojunction solar cells with exceptionally high performance. *Acc. Chem. Res.* **43**, 1227–1236 (2010).
13. Li, Y. Molecular design of photovoltaic materials for polymer solar cells: toward suitable electronic energy levels and broad absorption. *Acc. Chem. Res.* **45**, 723–733 (2012).
14. Chen, Y., Wan, X. & Long, G. High performance photovoltaic applications using solution-processed small molecules. *Acc. Chem. Res.* **46**, 2645–2655 (2013).
15. Liao, S., Jhuo, H., Cheng, Y. & Chen, S. Fullerene derivative-doped zinc oxide nanofilm as the cathode of inverted polymer solar cells with low-bandgap polymer (PTB7-Th) for high performance. *Adv. Mater.* **25**, 4766–4771 (2013).
16. Zhao, J. et al. Efficient organic solar cells processed from hydrocarbon solvents. *Nat. Energy* **1**, 15027 (2016).
17. Li, M. et al. Solution-processed organic tandem solar cells with power conversion efficiencies > 12%. *Nat. Photonics* **11**, 85–90 (2017).
18. Distler, A. et al. The effect of PCBM dimerization on the performance of bulk heterojunction solar cells. *Adv. Energy Mater.* **4**, 1300693 (2014).
19. Bloking, J. T. et al. Comparing the device physics and morphology of polymer solar cells employing fullerenes and non-fullerene acceptors. *Adv. Energy Mater.* **4**, 1301426 (2013).
20. Jinnai, S. et al. Electron-accepting π-conjugated systems for organic photovoltaics: influence of structural modification on molecular orientation at donor–acceptor interfaces. *Chem. Mater.* **28**, 1705–1713 (2016).
21. Su, G. et al. Linking morphology and performance of organic solar cells based on decacyclene triimide acceptors. *J. Mater. Chem. A* **2**, 1781–1789 (2014).
22. Savoie, B. M. et al. Mesoscale molecular network formation in amorphous organic materials. *Proc. Natl Acad. Sci. USA* **111**, 10055–10060 (2014).
23. Tang, C. W. Two-layer organic photovoltaic cell. *Appl. Phys. Lett.* **48**, 183–185 (1986).
24. Halls, J. J. M. et al. Efficient photodiodes from interpenetrating polymer networks. *Nature* **376**, 498–500 (1995).
25. Yu, G. & Heeger, A. J. Charge separation and photovoltaic conversion in polymer composites with internal donor/acceptor heterojunctions. *J. Appl. Phys.* **78**, 4510–4515 (1995).
26. Anthony, J. E. Small-molecule, nonfullerene acceptors for polymer bulk heterojunction organic photovoltaics. *Chem. Mater.* **23**, 583–590 (2011).
27. Sonar, P., Lim, J. P. F. & Chan, K. L. Organic non-fullerene acceptors for organic photovoltaics. *Energy Environ. Sci.* **4**, 1558–1574 (2011).
28. Li, C. & Wonneberger, H. Perylene imides for organic photovoltaics: yesterday, today, and tomorrow. *Adv. Mater.* **24**, 613–636 (2012).
29. Guo, X., Facchetti, A. & Marks, T. J. Imide- and amide-functionalized polymer semiconductors. *Chem. Rev.* **114**, 8943–9021 (2014).
30. Lin, Y. & Zhan, X. Non-fullerene acceptors for organic photovoltaics: an emerging horizon. *Mater. Horiz.* **1**, 470–488 (2014).
31. Lin, Y. & Zhan, X. Designing efficient non-fullerene acceptors by tailoring extended fused-rings with electron-deficient groups. *Adv. Energy Mater.* **5**, 1501063 (2015).
32. Nielsen, C. B., Holliday, S., Chen, H., Cryer, S. J. & McCulloch, I. Non-fullerene electron acceptors for use in organic solar cells. *Acc. Chem. Res.* **48**, 2803–2812 (2015).
33. Kang, H. et al. From fullerene-polymer to all-polymer solar cells: the importance of molecular packing, orientation, and morphology control. *Acc. Chem. Res.* **49**, 2424–2434 (2016).
34. Lin, Y. & Zhan, X. Oligomer molecules for efficient organic photovoltaics. *Acc. Chem. Res.* **49**, 175–183 (2016).
35. Zhao, W. et al. Molecular optimization enables over 13% efficiency in organic solar cells. *J. Am. Chem. Soc.* **139**, 7148–7151 (2017).
36. Cui, Y. et al. Fine-tuned photoactive and interconnection layers for achieving over 13% efficiency in a fullerene-free tandem organic solar cell. *J. Am. Chem. Soc.* **139**, 7302–7309 (2017).
37. Kumari, T., Lee, S. M., Kang, S. H., Chen, S. & Yang, C. Ternary solar cells with a mixed face-on and edge-on orientation enable an unprecedented efficiency of 12.1%. *Energy Environ. Sci.* **10**, 258–265 (2017).
38. Kwon, O. K., Park, J.-H., Kim, D. W., Park, S. K. & Park, S. Y. An all-small-molecule organic solar cell with high efficiency nonfullerene acceptor. *Adv. Mater.* **27**, 1951–1956 (2015).
39. Patil, Y., Misra, R., Keshtov, M. L. & Sharma, G. D. Small molecule carbazole-based diketopyrrolopyrroles with tetracyanobutadiene acceptor unit as a non-fullerene acceptor for bulk heterojunction organic solar cells. *J. Mater. Chem. A* **5**, 3311–3319 (2017).
40. Shu, Y. et al. A survey of electron-deficient pentacenes as acceptors in polymer bulk heterojunction solar cells. *Chem. Sci.* **2**, 363–368 (2011).
41. Li, H. et al. Beyond fullerenes: design of nonfullerene acceptors for efficient organic photovoltaics. *J. Am. Chem. Soc.* **136**, 14589–14597 (2014).
42. Dang, M. et al. Bis(tri-*n*-alkylsilyl oxide) silicon phthalocyanines: a start to establishing a structure property relationship as both ternary additives and non-fullerene electron acceptors in bulk heterojunction organic photovoltaic devices. *J. Mater. Chem. A* **5**, 12168–12182 (2017).
43. Long, X. et al. Polymer acceptor based on double B←N bridged bipyridine (BNBP) unit for high-efficiency all-polymer solar cells. *Adv. Mater.* **28**, 6504–6508 (2016).
44. Cnops, K. et al. 8.4% Efficient fullerene-free organic solar cells exploiting long-range exciton energy transfer. *Nat. Commun.* **5**, 3406 (2014).
45. Zhan, X. et al. Rylene and related diimides for organic electronics. *Adv. Mater.* **23**, 268–284 (2011).
46. Suraru, S. L. & Wurthner, F. Strategies for the synthesis of functional naphthalene diimides. *Angew. Chem. Int. Ed.* **53**, 7428–7448 (2014).
47. Pho, T. V., Toma, F. M., Chabinyc, M. L. & Wudl, F. Self-assembling decacyclene triimides prepared through a regioselective hextuple Friedel–Crafts carbamylation. *Angew. Chem. Int. Ed.* **52**, 1446–1451 (2013).
48. Li, H. et al. Tetraazabenzodifluoranthene diimides: building blocks for solution-processable n-type organic semiconductors. *Angew. Chem. Int. Ed.* **52**, 5513–5517 (2013).
49. Li, H. et al. Fine-tuning the 3D structure of nonfullerene electron acceptors toward high-performance polymer solar cells. *Adv. Mater.* **27**, 3266–3272 (2015).
50. Shoaee, S. et al. Acceptor energy level control of charge photogeneration in organic donor/acceptor blends. *J. Am. Chem. Soc.* **132**, 12919–12926 (2010).
51. Shoaee, S. et al. Charge photogeneration in polythiophene–perylene diimide blend films. *Chem. Commun.* 5445–5447 (2009).
52. Shin, W. S. et al. Effects of functional groups at perylene diimide derivatives on organic photovoltaic device application. *J. Mater. Chem.* **16**, 384–390 (2006).
53. Schubert, A. et al. Ultrafast exciton self-trapping upon geometry deformation in perylene-based molecular aggregates. *J. Phys. Chem. Lett.* **4**, 792–796 (2013).
54. Sharenko, A. et al. A high-performing solution-processed small molecule:perylene diimide bulk heterojunction solar cell. *Adv. Mater.* **25**, 4403–4406 (2013).
55. Hartnett, P. E. et al. Slip-stacked perylenediimides as an alternative strategy for high efficiency nonfullerene acceptors in organic photovoltaics. *J. Am. Chem. Soc.* **136**, 16345–16356 (2014).

56. Liu, J. et al. Fast charge separation in a non-fullerene organic solar cell with a small driving force. *Nat. Energy* **1**, 16089 (2016).
57. Langhals, H. & Jona, W. Intense dyes through chromophore–chromophore interactions: bi- and trichromophoric perylene-3,4:9,10-bis(dicarboximide)s. *Angew. Chem. Int. Ed.* **37**, 952–955 (1998).
58. Langhals, H. & Saulich, S. Bichromophoric perylene derivatives: energy transfer from non-fluorescent chromophores. *Chem. Eur. J.* **8**, 5630–5643 (2002).
59. Holman, M. W., Yan, P., Adams, D. M., Westenhoff, S. & Silva, C. Ultrafast spectroscopy of the solvent dependence of electron transfer in a perylenebisimide dimer. *J. Phys. Chem. A* **109**, 8548–8552 (2005).
60. Wilson, T. M., Tauber, M. J. & Wasielewski, M. R. Toward an n-type molecular wire: electron hopping within linearly linked perylenediimide oligomers. *J. Am. Chem. Soc.* **131**, 8952–8957 (2009).
61. Rajaram, S., Shivanna, R., Kandappa, S. K. & Narayan, K. S. Nonplanar perylene diimides as potential alternatives to fullerenes in organic solar cells. *J. Phys. Chem. Lett.* **3**, 2405–2408 (2012).
62. Shivanna, R. et al. Charge generation and transport in efficient organic bulk heterojunction solar cells with a perylene acceptor. *Energy Environ. Sci.* **7**, 435–441 (2014).
63. Ye, L. et al. Enhanced efficiency in fullerene-free polymer solar cell by incorporating fine-designed donor and acceptor materials. *ACS Appl. Mater. Interfaces* **7**, 9274–9280 (2015).
64. Liang, N. et al. Perylene diimide trimers based bulk heterojunction organic solar cells with efficiency over 7%. *Adv. Energy Mater.* **6**, 1600060 (2016).
65. Jiang, W. et al. Bay-linked perylene bisimides as promising non-fullerene acceptors for organic solar cells. *Chem. Commun.* **50**, 1024–1026 (2014).
66. Zang, Y. et al. Integrated molecular, interfacial, and device engineering towards high-performance non-fullerene based organic solar cells. *Adv. Mater.* **26**, 5708–5714 (2014).
67. Ye, L. et al. Toward efficient non-fullerene polymer solar cells: selection of donor polymers. *Org. Electron.* **17**, 295–303 (2015).
68. Wu, C. et al. Influence of molecular geometry of perylene diimide dimers and polymers on bulk heterojunction morphology toward high-performance nonfullerene polymer solar cells. *Adv. Funct. Mater.* **25**, 5326–5332 (2015).
69. Sun, D. et al. Non-fullerene-acceptor-based bulk-heterojunction organic solar cells with efficiency over 7%. *J. Am. Chem. Soc.* **137**, 11156–11162 (2015).
70. Meng, D. et al. High-performance solution-processed non-fullerene organic solar cells based on selenophene-containing perylene bisimide acceptor. *J. Am. Chem. Soc.* **138**, 375–380 (2016).
71. Fan, Y. et al. Comparison of the optical and electrochemical properties of bi(perylene diimide)s linked through ortho and bay positions. *ACS Omega* **2**, 377–385 (2017).
72. Yan, Q., Zhou, Y., Zheng, Y., Pei, J. & Zhao, D. Towards rational design of organic electron acceptors for photovoltaics: a study based on perylenediimide derivatives. *Chem. Sci.* **4**, 4389–4394 (2013).
73. Zhang, X. et al. A potential perylene diimide dimer-based acceptor material for highly efficient solution-processed non-fullerene organic solar cells with 4.03% efficiency. *Adv. Mater.* **25**, 5791–5797 (2013).
74. Lin, Y. et al. A star-shaped perylene diimide electron acceptor for high-performance organic solar cells. *Adv. Mater.* **26**, 5137–5142 (2014).
75. Duan, Y. et al. Pronounced effects of a triazine core on photovoltaic performance-efficient organic solar cells enabled by a PDI trimer-based small molecular acceptor. *Adv. Mater.* **29**, 1605115 (2017).
76. Lin, H. et al. Reduced intramolecular twisting improves the performance of 3D molecular acceptors in non-fullerene organic solar cells. *Adv. Mater.* **28**, 8546–8551 (2016).
77. Wu, Q., Zhao, D., Schneider, A. M., Chen, W. & Yu, L. Covalently bound clusters of alpha-substituted PDI–rival electron acceptors to fullerene for organic solar cells. *J. Am. Chem. Soc.* **138**, 7248–7251 (2016).
78. Chen, W. et al. A perylene diimide (PDI)-based small molecule with tetrahedral configuration as a non-fullerene acceptor for organic solar cells. *J. Mater. Chem. C* **3**, 4698–4705 (2015).
79. Zhong, Y. et al. Efficient organic solar cells with helical perylene diimide electron acceptors. *J. Am. Chem. Soc.* **136**, 15215–15221 (2014).
80. Zhong, Y. et al. Molecular helices as electron acceptors in high-performance bulk heterojunction solar cells. *Nat. Commun.* **6**, 8242 (2015).
81. Zhong, H. et al. Rigidifying nonplanar perylene diimides by ring fusion toward geometry-tunable acceptors for high-performance fullerene-free solar cells. *Adv. Mater.* **28**, 951–958 (2016).
82. Meng, D. et al. Three-bladed rylene propellers with three-dimensional network assembly for organic electronics. *J. Am. Chem. Soc.* **138**, 10184–10190 (2016).
83. Facchetti, A. Polymer donor–polymer acceptor (all-polymer) solar cells. *Mater. Today* **16**, 123–132 (2013).
84. Deshmukh, K. D. et al. Performance, morphology and photophysics of high open-circuit voltage, low band gap all-polymer solar cells. *Energy Environ. Sci.* **8**, 332–342 (2015).
85. Lu, L. et al. Recent advances in bulk heterojunction polymer solar cells. *Chem. Rev.* **115**, 12666–12731 (2015).
86. Moore, J. R. et al. Polymer blend solar cells based on a high-mobility naphthalenediimide-based polymer acceptor: device physics, photophysics and morphology. *Adv. Energy Mater.* **1**, 230–240 (2011).
87. Guo, Y. et al. Improved performance of all-polymer solar cells enabled by naphthodiperylenetetraimide-based polymer acceptor. *Adv. Mater.* **29**, 1700309 (2017).
88. Gao, L. et al. All-polymer solar cells based on absorption-complementary polymer donor and acceptor with high power conversion efficiency of 8.27%. *Adv. Mater.* **28**, 1884–1890 (2016).
89. Fan, B. et al. Optimisation of processing solvent and molecular weight for the production of green-solvent-processed all-polymer solar cells with a power conversion efficiency over 9%. *Energy Environ. Sci.* **10**, 1243–1251 (2017).
90. Zhan, X. et al. A high-mobility electron-transport polymer with broad absorption and its use in field-effect transistors and all-polymer solar cells. *J. Am. Chem. Soc.* **129**, 7246–7247 (2007).
91. Tan, Z. et al. Efficient all-polymer solar cells based on blend of tris(thienylenevinylene)-substituted polythiophene and poly[perylene diimide-*alt*-bis(dithienothiophene)]. *Appl. Phys. Lett.* **93**, 073309 (2008).
92. Zhan, X. et al. Copolymers of perylene diimide with dithienothiophene and dithienopyrrole as electron-transport materials for all-polymer solar cells and field-effect transistors. *J. Mater. Chem.* **19**, 5794–5803 (2009).
93. Huang, J. et al. Photoinduced intramolecular electron transfer in conjugated perylene bisimide-dithienothiophene systems: a comparative study of a small molecule and a polymer. *J. Phys. Chem. A* **113**, 5039–5046 (2009).
94. Cheng, P. et al. Binary additives synergistically boost the efficiency of all-polymer solar cells up to 3.45%. *Energy Environ. Sci.* **7**, 1351–1356 (2014).
95. Cheng, P., Yan, C., Li, Y., Ma, W. & Zhan, X. Diluting concentrated solution: a general, simple and effective approach to enhance efficiency of polymer solar cells. *Energy Environ. Sci.* **8**, 2357–2364 (2015).
96. Hou, J., Zhang, S., Chen, T. & Yang, Y. A new n-type low bandgap conjugated polymer P-co-CDT: synthesis and excellent reversible electrochemical and electrochromic properties. *Chem. Commun.* 6034–6036 (2008).
97. Zhou, E., Tajima, K., Yang, C. & Hashimoto, K. Band gap and molecular energy level control of perylene diimide-based donor–acceptor copolymers for all-polymer solar cells. *J. Mater. Chem.* **20**, 2362–2368 (2010).
98. Zhou, E. et al. All-polymer solar cells from perylene diimide based copolymers: material design and phase separation control. *Angew. Chem. Int. Ed.* **50**, 2799–2803 (2011).
99. Hu, X. et al. Synthesis and photovoltaic properties of n-type conjugated polymers alternating 2,7-carbazole and arylene diimides. *Sol. Energy Mater. Sol. Cells* **103**, 157–163 (2012).
100. Zhou, Y. et al. New polymer acceptors for organic solar cells: the effect of regio-regularity and device configuration. *J. Mater. Chem. A* **1**, 6609–6613 (2013).
101. Zhou, Y. et al. High performance all-polymer solar cell via polymer side-chain engineering. *Adv. Mater.* **26**, 3767–3772 (2014).
102. Diao, Y. et al. Flow-enhanced solution printing of all-polymer solar cells. *Nat. Commun.* **6**, 7955 (2015).
103. Guo, Y. et al. A vinylene-bridged perylenediimide-based polymeric acceptor enabling efficient all-polymer solar cells processed under ambient conditions. *Adv. Mater.* **28**, 8483–8489 (2016).
104. Wurthner, F. et al. Preparation and characterization of regioisomerically pure 1,7-disubstituted perylene bisimide dyes. *J. Org. Chem.* **69**, 7933–7939 (2004).
105. Yan, H. et al. A high-mobility electron-transporting polymer for printed transistors. *Nature* **457**, 679–686 (2009).
106. Li, Z. et al. High performance all-polymer solar cells by synergistic effects of fine-tuned crystallinity and solvent annealing. *J. Am. Chem. Soc.* **138**, 10935–10944 (2016).
107. Jung, J. et al. Fluoro-substituted n-type conjugated polymers for additive-free all-polymer bulk heterojunction solar cells with high power conversion efficiency of 6.71%. *Adv. Mater.* **27**, 3310–3317 (2015).
108. Earmme, T., Hwang, Y., Murari, N. M., Subramaniyan, S. & Jenekhe, S. A. All-polymer solar cells with 3.3% efficiency based on naphthalene diimide-selenophene copolymer acceptor. *J. Am. Chem. Soc.* **135**, 14960–14963 (2013).
109. Earmme, T., Hwang, Y., Subramaniyan, S. & Jenekhe, S. A. All-polymer bulk heterojuction solar cells with 4.8% efficiency achieved by solution processing from a co-solvent. *Adv. Mater.* **26**, 6080–6085 (2014).
110. Hwang, Y., Courtright, B. A., Ferreira, A. S., Tolbert, S. H. & Jenekhe, S. A. 7.7% Efficient all-polymer solar cells. *Adv. Mater.* **27**, 4578–4584 (2015).
111. Hwang, Y., Ren, G., Murari, N. M. & Jenekhe, S. A. n-Type naphthalene diimide–biselenophene copolymer for all-polymer bulk heterojunction solar cells. *Macromolecules* **45**, 9056–9062 (2012).
112. Lee, C. et al. High-performance all-polymer solar cells via side-chain engineering of the polymer acceptor: the importance of the polymer packing structure and the nanoscale blend morphology. *Adv. Mater.* **27**, 2466–2471 (2015).
113. Lee, W. et al. Side chain optimization of naphthalenediimide–bithiophene-based polymers to enhance the electron mobility and the performance in all-polymer solar cells. *Adv. Funct. Mater.* **26**, 1543–1553 (2016).
114. Choi, J. et al. Importance of electron transport ability in naphthalene diimide-based polymer acceptors for high-performance, additive-free, all-polymer solar cells. *Chem. Mater.* **27**, 5230–5237 (2015).
115. Hwang, Y., Earmme, T., Courtright, B. A., Eberle, F. N. & Jenekhe, S. A. n-Type semiconducting naphthalene diimide-perylene diimide copolymers: controlling crystallinity, blend morphology, and compatibility toward high-performance all-polymer solar cells. *J. Am. Chem. Soc.* **137**, 4424–4434 (2015).
116. Wu, J., Cheng, S., Cheng, Y. & Hsu, C. Donor–acceptor conjugated polymers based on multifused ladder-type arenes for organic solar cells. *Chem. Soc. Rev.* **44**, 1113–1154 (2015).
117. Han, G., Guo, Y., Song, X., Wang, Y. & Yi, Y. Terminal π–π stacking determines three-dimensional molecular packing and isotropic charge transport in an A–π–A electron acceptor for non-fullerene organic solar cells. *J. Mater. Chem. C* **5**, 4852–4857 (2017).
118. Kim, Y., Song, C. E., Moon, S.-J. & Lim, E. Effect of dye end groups in non-fullerene fluorene- and carbazole-based small molecule acceptors on photovoltaic performance. *RSC Adv.* **5**, 62739–62746 (2015).
119. Wang, K. et al. π-Bridge-independent 2-(benzo[*c*][1,2,5]thiadiazol-4-ylmethylene)malononitrile-substituted nonfullerene acceptors for efficient bulk heterojunction solar cells. *Chem. Mater.* **28**, 2200–2208 (2016).
120. Zhang, G. et al. Efficient nonfullerene polymer solar cells enabled by a novel wide bandgap small molecular acceptor. *Adv. Mater.* **29**, 1606054 (2017).
121. Stoltzfus, D. M., Clulow, A. J., Jin, H., Burn, P. L. & Gentle, I. R. Impact of dimerization on phase separation and crystallinity in bulk heterojunction films containing non-fullerene acceptors. *Macromolecules* **49**, 4404–4415 (2016).
122. Lin, Y. et al. Structure evolution of oligomer fused-ring electron acceptors toward high efficiency of as-cast polymer solar cells. *Adv. Energy Mater.* **6**, 1600854 (2016).
123. Kan, B. et al. Small-molecule acceptor based on the heptacyclic benzodi(cyclopentadithiophene) unit for highly efficient nonfullerene organic solar cells. *J. Am. Chem. Soc.* **139**, 4929–4934 (2017).

124. Lin, Y. et al. An electron acceptor challenging fullerenes for efficient polymer solar cells. *Adv. Mater.* **27**, 1170–1174 (2015).
125. Dai, S. et al. Fused nonacyclic electron acceptors for efficient polymer solar cells. *J. Am. Chem. Soc.* **139**, 1336–1343 (2017).
126. Li, Y. et al. Non-fullerene acceptor with low energy loss and high external quantum efficiency: towards high performance polymer solar cells. *J. Mater. Chem. A* **4**, 5890–5897 (2016).
127. Wang, W. et al. Fused hexacyclic nonfullerene acceptor with strong near-infrared absorption for semitransparent organic solar cells with 9.77% efficiency. *Adv. Mater.* **29**, 1701308 (2017).
128. Zhao, W. et al. Fullerene-free polymer solar cells with over 11% efficiency and excellent thermal stability. *Adv. Mater.* **28**, 4734–4739 (2016).
129. Bin, H. et al. 11.4% Efficiency non-fullerene polymer solar cells with trialkylsilyl substituted 2D-conjugated polymer as donor. *Nat. Commun.* **7**, 13651 (2016).
130. Yang, Y. et al. Side-chain isomerization on an n-type organic semiconductor ITIC acceptor makes 11.77% high efficiency polymer solar cells. *J. Am. Chem. Soc.* **138**, 15011–15018 (2016).
131. Zuo, L. et al. High-efficiency nonfullerene organic solar cells with a parallel tandem configuration. *Adv. Mater.* **29**, 1702547 (2017).
132. Zhu, J. et al. Naphthodithiophene-based nonfullerene acceptor for high-performance organic photovoltaics: effect of extended conjugation. *Adv. Mater.* **30**, 1704713 (2017).
133. Li, Y. et al. A fused-ring based electron acceptor for efficient non-fullerene polymer solar cells with small HOMO offset. *Nano Energy* **27**, 430–438 (2016).
134. Kronenberg, N. M. et al. Bulk heterojunction organic solar cells based on merocyanine colorants. *Chem. Commun.* 6489–6491 (2008).
135. Wu, Y. et al. A planar electron acceptor for efficient polymer solar cells. *Energy Environ. Sci.* **8**, 3215–3221 (2015).
136. Cheng, P. et al. Realizing small energy loss of 0.55 eV, high open-circuit voltage > 1 V and high efficiency > 10% in fullerene-free polymer solar cells via energy driver. *Adv. Mater.* **29**, 1605216 (2017).
137. Xiao, B. et al. Achievement of high V_{OC} of 1.02 V for P3HT-based organic solar cell using a benzotriazole-containing non-fullerene acceptor. *Adv. Energy Mater.* **7**, 1602269 (2017).
138. Liu, F. et al. A thieno[3,4-*b*]thiophene-based non-fullerene electron acceptor for high-performance bulk-heterojunction organic solar cells. *J. Am. Chem. Soc.* **138**, 15523–15526 (2016).
139. Jia, B. et al. Rhodanine flanked indacenodithiophene as non-fullerene acceptor for efficient polymer solar cells. *Sci. China Chem.* **60**, 257–263 (2017).
140. Lin, Y. et al. A twisted dimeric perylene diimide electron acceptor for efficient organic solar cells. *Adv. Energy Mater.* **4**, 1400420 (2014).
141. Li, S. et al. Energy-level modulation of small-molecule electron acceptors to achieve over 12% efficiency in polymer solar cells. *Adv. Mater.* **28**, 9423–9429 (2016).
142. Yao, H. et al. Achieving highly efficient nonfullerene organic solar cells with improved intermolecular interaction and open-circuit voltage. *Adv. Mater.* **29**, 1700254 (2017).
143. Xie, D. et al. A novel thiophene-fused ending group enabling an excellent small molecule acceptor for high-performance fullerene-free polymer solar cells with 11.8% efficiency. *Sol. RRL* **1**, 1700044 (2017).
144. Feng, H. et al. An A-D-A type small-molecule electron acceptor with end-extended conjugation for high performance organic solar cells. *Chem. Mater.* **29**, 7908–7917 (2017).
145. Lin, Y. et al. High-performance electron acceptor with thienyl side chains for organic photovoltaics. *J. Am. Chem. Soc.* **138**, 4955–4961 (2016).
146. Zhao, F. et al. Single-junction binary-blend nonfullerene polymer solar cells with 12.1% efficiency. *Adv. Mater.* **29**, 1700144 (2017).
147. Wang, J. et al. Enhancing performance of nonfullerene acceptors via side-chain conjugation strategy. *Adv. Mater.* **29**, 1702125 (2017).
148. Lin, Y. et al. A facile planar fused-ring electron acceptor for as-cast polymer solar cells with 8.71% efficiency. *J. Am. Chem. Soc.* **138**, 2973–2976 (2016).
149. Lin, Y. et al. Mapping polymer donors toward high-efficiency fullerene free organic solar cells. *Adv. Mater.* **29**, 1604155 (2017).
150. Holliday, S. et al. High-efficiency and air-stable P3HT-based polymer solar cells with a new non-fullerene acceptor. *Nat. Commun.* **7**, 11585 (2016).
151. Baran, D. et al. Reducing the efficiency–stability–cost gap of organic photovoltaics with highly efficient and stable small molecule acceptor ternary solar cells. *Nat. Mater.* **16**, 363–369 (2017).
152. Lin, Y. et al. High-performance fullerene-free polymer solar cells with 6.31% efficiency. *Energy Environ. Sci.* **8**, 610–616 (2015).
153. Bai, H. et al. An electron acceptor based on indacenodithiophene and 1,1-dicyanomethylene-3-indanone for fullerene-free organic solar cells. *J. Mater. Chem. A* **3**, 1910–1914 (2015).
154. Yan, C. et al. Enhancing performance of non-fullerene organic solar cells via side chain engineering of fused-ring electron acceptors. *Dyes Pigm.* **139**, 627–634 (2017).
155. Yao, H. et al. Design and synthesis of a low bandgap small molecule acceptor for efficient polymer solar cells. *Adv. Mater.* **28**, 8283–8287 (2016).
156. Yao, H. et al. Design, synthesis, and photovoltaic characterization of a small molecular acceptor with an ultra-narrow band gap. *Angew. Chem. Int. Ed.* **56**, 3045–3049 (2017).
157. Gao, L. et al. High-efficiency nonfullerene polymer solar cells with medium bandgap polymer donor and narrow bandgap organic semiconductor acceptor. *Adv. Mater.* **28**, 8288–8295 (2016).
158. Bin, H. et al. Non-fullerene polymer solar cells based on alkylthio and fluorine substituted 2D-conjugated polymers reach 9.5% efficiency. *J. Am. Chem. Soc.* **138**, 4657–4664 (2016).
159. Ye, L. et al. Manipulating aggregation and molecular orientation in all-polymer photovoltaic cells. *Adv. Mater.* **27**, 6046–6054 (2015).
160. Yao, J. et al. Quantifying losses in open-circuit voltage in solution-processable solar cells. *Phys. Rev. Appl.* **4**, 014020 (2015).
161. Scharber, M. C. et al. Design rules for donors in bulk-heterojunction solar cells — towards 10% energy-conversion efficiency. *Adv. Mater.* **18**, 789–794 (2006).
162. Clarke, T. M. & Durrant, J. R. Charge photogeneration in organic solar cells. *Chem. Rev.* **110**, 6736–6767 (2010).
163. Veldman, D., Meskers, S. C. J. & Janssen, R. A. J. The energy of charge-transfer states in electron donor–acceptor blends: insight into the energy losses in organic solar cells. *Adv. Funct. Mater.* **19**, 1939–1948 (2009).
164. Li, W., Hendriks, K. H., Furlan, A., Wienk, M. M. & Janssen, R. A. High quantum efficiencies in polymer solar cells at energy losses below 0.6 eV. *J. Am. Chem. Soc.* **137**, 2231–2234 (2015).
165. Kawashima, K., Tamai, Y., Ohkita, H., Osaka, I. & Takimiya, K. High-efficiency polymer solar cells with small photon energy loss. *Nat. Commun.* **6**, 10085 (2015).
166. Ran, N. et al. Harvesting the full potential of photons with organic solar cells. *Adv. Mater.* **28**, 1482–1488 (2016).
167. Wang, C. et al. Low band gap polymer solar cells with minimal voltage losses. *Adv. Energy Mater.* **6**, 1600148 (2016).
168. Baran, D. et al. Reduced voltage losses yield 10% efficient fullerene free organic solar cells with > 1 V open circuit voltages. *Energy Environ. Sci.* **9**, 3783–3793 (2016).
169. Benduhn, J. et al. Intrinsic non-radiative voltage losses in fullerene-based organic solar cells. *Nat. Energy* **2**, 17053 (2017).
170. Bartesaghi, D. et al. Competition between recombination and extraction of free charges determines the fill factor of organic solar cells. *Nat. Commun.* **6**, 7083 (2015).
171. Collins, B. A. et al. Absolute measurement of domain composition and nanoscale size distribution explains performance in PTB7:PC_{71}BM solar cells. *Adv. Energy Mater.* **3**, 65–74 (2013).
172. Liu, Y. et al. Aggregation and morphology control enables multiple cases of high-efficiency polymer solar cells. *Nat. Commun.* **5**, 5293 (2014).
173. Mukherjee, S., Proctor, C. M., Bazan, G. C., Nguyen, T. Q. & Ade, H. Significance of average domain purity and mixed domains on the photovoltaic performance of high-efficiency solution-processed small-molecule BHJ solar cells. *Adv. Energy Mater.* **5**, 1500877 (2015).
174. Jao, M., Liao, H. & Su, W. Achieving a high fill factor for organic solar cells. *J. Mater. Chem. A* **4**, 5784–5801 (2016).
175. Xie, Z. & Wurthner, F. Hybrid photoconductive cathode interlayer materials composed of perylene bisimide photosensitizers and zinc oxide for high performance polymer solar cells. *Adv. Energy Mater.* **7**, 1602573 (2017).
176. Cheng, P. & Zhan, X. Stability of organic solar cells: challenges and strategies. *Chem. Soc. Rev.* **45**, 2544–2582 (2016).
177. Bai, H. et al. Nonfullerene acceptors based on extended fused rings flanked with benzothiadiazolylmethylenemalononitrile for polymer solar cells. *J. Mater. Chem. A* **3**, 20758–20766 (2015).

Acknowledgements
X.Z. acknowledges support from the National Natural Science Foundation of China (Grant Nos 21734001 and 51761165023). S.B. and S.R.M. acknowledge support from the US Department of the Navy, Office of Naval Research (Grant No. N00014-14-1-0580 (CAOP MURI)). Z.W. acknowledges support from the National Natural Science Foundation of China (Grant No. 21734009). H.Y. acknowledges support from the National Basic Research Program of China (Grant Nos 2013CB834701 and 2014CB643501) and the Hong Kong Innovation and Technology Commission (Grant Nos ITC-CNERC14SC01 and ITS/083/15). A.K.-Y.J. acknowledges support from the US Office of Naval Research (Grant No. N00014-17-1-2201) and the Asian Office of Aerospace R&D (Grant No. FA2386-15-1-4106).

Author contributions
C.Y., S.B., Z.W., H.Y. and X.Z. researched data for the article. All authors contributed to the writing and editing of the article before submission.

Competing interests
The authors declare no competing interests.

Publisher's note
Springer Nature remains neutral with regard to jurisdictional claims in published maps and institutional affiliations.

How to cite this article
Yan, C. et al. Non-fullerene acceptors for organic solar cells. *Nat. Rev. Mater.* **3**, 18003 (2018).